

1
2
3
4
5
6
7
8
9
10
11
12
13
14
15
16
17
18
19
20
21
22
23
24

Variability and past long-term changes of brominated VSLs at the tropical tropopause

Susann Tegtmeier^{1*}, Elliot Atlas², Birgit Quack¹, Franziska Ziska¹, and Kirstin Krüger³

¹GEOMAR Helmholtz Centre for Ocean Research Kiel, Kiel, Germany

*Now at: Institute of Space and Atmospheric Studies, University of Saskatchewan, Saskatoon, Canada

²Rosenstiel School of Marine and Atmospheric Science, University of Miami, Miami, Florida, USA

³Meteorology and Oceanography Section, Department of Geosciences, University of Oslo, Oslo, Norway

1 **Abstract**

2

3 Halogenated very short-lived substances (VSLS), such as bromoform (CHBr₃), can be
4 transported to the stratosphere and contribute to the halogen loading and ozone depletion. Given
5 their highly variable emission rates and their short atmospheric lifetimes, the exact amount as
6 well as the tempo-spatial variability of their contribution to the stratospheric halogen loading is
7 still uncertain. We combine observational data sets with Lagrangian atmospheric modelling in
8 order to analyse the spatial and temporal variability of the CHBr₃ injection into the stratosphere
9 for the time period 1979-2013. Regional maxima with mixing ratios of up to 0.4-0.5 ppt at 17
10 km altitude are diagnosed to be over Central America (1) and over the Maritime Continent/West
11 Pacific (2), both of which are confirmed by high-altitude aircraft campaigns. The CHBr₃
12 maximum over Central America is caused by the co-occurrence of convectively driven short
13 transport time scales and strong regional sources, which in conjunction drive the seasonality of
14 CHBr₃ injection. Model results at a daily resolution reveal isolated, exceptionally high CHBr₃
15 values in this region which are confirmed by aircraft measurements during the ACCENT
16 campaign and do not occur in spatially or temporally averaged model fields. CHBr₃ injection
17 over the West Pacific is centred south of the equator due to strong oceanic sources underneath
18 prescribed by the here applied bottom-up emission inventory. The globally largest CHBr₃
19 mixing ratios at the cold point level of up to 0.6 ppt are diagnosed to occur over the region of
20 India, Bay of Bengal and Arabian Sea (3), however, no data from aircraft campaigns are
21 available to confirm this finding. Interannual variability of stratospheric CHBr₃ injection of 10-
22 20% is to a large part driven by the variability of coupled ocean-atmosphere circulation systems.
23 Long-term changes, on the other hand, correlate with the regional SST trends resulting in
24 positive trends of stratospheric CHBr₃ injection over the West Pacific and Asian monsoon
25 region and negative trends over the East Pacific. For the tropical mean, these opposite regional
26 trends balance each other out resulting in a relatively weak positive trend of 0.017±0.012 ppt
27 Br/decade for 1979-2013, corresponding 3% Br/decade. The overall contribution of CHBr₃
28 together with CH₂Br₂ to the stratospheric halogen loading accounts for 4.7 ppt Br, in good
29 agreement with existing studies, with 50%/50% being injected in form of source and product
30 gases, respectively.

31

1 **1 Introduction**

2

3 It has long been recognized that the depletion of stratospheric ozone over the last 30 years is
4 mainly caused by human-made chlorine- and bromine-containing substances, often referred to
5 as ozone-depleting substances (ODS) (Carpenter and Reimann et al., 2014). The Montreal
6 Protocol, crafted in 1987 to control the production and consumption of ODSs, has been very
7 successful in reducing the emission of the long-lived halocarbons. As a result, the overall
8 abundance of ODS in the atmosphere has been decreasing since the beginning of the 21st
9 century and the stratospheric ozone layer is expected to recover around the middle of the 21st
10 century (Austin and Butchart, 2003; Carpenter and Reimann et al., 2014, Salawitch et al., 2019).

11 In contrast to long-lived halocarbons, the so-called Very Short-Lived Substances (VSLS) with
12 chemical lifetimes of less than 6 months (e.g. Ko and Poulet et al., 2003), are not controlled by
13 the Montreal Protocol and are even suggested to increase in the future (e.g., Pyle et al., 2007;
14 Tegtmeier et al., 2015; Ziska et al., 2017). Brominated VSLS are primarily of natural origin
15 emitted by oceanic macroalgae and phytoplankton (e.g., Quack and Wallace, 2003). Over the
16 last years there has been increasing evidence from observational (e.g., Dorf et al., 2008; Sioris
17 et al., 2006; McLinden et al., 2010; Brinckmann et al., 2012) and modelling (e.g., Warwick et
18 al. 2006; Liang et al., 2010; Hossaini et al., 2012b; Tegtmeier et al., 2012; Hossaini et al., 2016)
19 studies that VSLS provide a significant contribution to stratospheric total bromine (Br_y).
20 Current estimates of this contribution are about 5 (3 - 7) ppt bromine (Engel and Rigby, 2018;
21 Navarro et al., 2015; Wales et al., 2018). The injection of VSLS into the stratosphere in form
22 of source gases (SGs) or inorganic product gases (PGs) depends strongly on the efficiency of
23 troposphere-stratosphere transport versus the degradation of the source gases (through
24 photochemical loss) and product gases (through wet deposition). In particular, the question of
25 heterogeneous release of bromine back to the gas phase, which determines the efficiency of wet
26 deposition as a sink for Br_y , is currently under discussion (e.g., Salawitch, 2006; Aschmann et
27 al., 2011, Fernandez et al., 2014, Schmidt et al., 2016). Once brominated VSLS have reached
28 the stratosphere in the form of SG or PG, they participate in ozone depletion at middle and high
29 latitudes (Braesicke et al., 2013; Yang et al., 2014; Sinnhuber and Meul, 2015). Through their
30 relatively large impact on ozone in the lower stratosphere, they contribute $-0.02Wm^{-2}$ to global
31 radiative forcing (Hossaini et al., 2015).

1 The most abundant bromine containing VSLS are bromoform (CHBr_3) and dibromomethane
2 (CH_2Br_2) with atmospheric lifetimes estimates ranging from 16 (50) days at the ocean surface
3 to 29 (400) days in the TTL for CHBr_3 (CH_2Br_2) (Hossaini et al., 2012b). Both gases have
4 potentially important source regions in tropical, subtropical and shelf waters (e.g., Butler et al.,
5 2007; Quack et al., 2007). The emissions of brominated VSLS from the ocean into the
6 atmosphere can be derived based on their concentration gradient between water and air, wind
7 speed, sea surface temperature and salinity (e.g. Nightingale et al. 2000; Quack and Wallace
8 2003; Ziska et al. 2013). The magnitude and distribution of brominated VSLS emissions are
9 poorly constrained given the sparse observational data base of their oceanic and atmospheric
10 concentrations (Ziska et al., 2013). Current emission inventories have been mostly derived via
11 the top-down approach by adjusting the estimated VSLS emissions in a global atmospheric
12 model to produce agreement of the model simulations with aircraft observations. For CHBr_3 ,
13 the current global top-down emissions range between 426 - 530 Gg Br/year (Liang et al., 2010;
14 Warwick et al., 2006, Ordonez et al., 2012), while the bottom-up approach based on statistical
15 gap filling of an observational data base suggests smaller global fluxes of 164-236 Gg Br/year
16 (Ziska et al., 2013). A recent oceanic modelling study taking into account source and sink
17 processes projects open ocean emissions of around 72 Gg Br/year in form of CHBr_3 , not
18 including the strong coastal sources (Stemmler et al., 2015). Quantitative evaluations of various
19 emission inventories demonstrated that the performance of the individual inventories depends
20 strongly on the region and model applied for the evaluation (Hossaini et al., 2013; Hossaini et
21 al., 2016).

22 Stratospheric injection of trace gases with lifetimes of days to weeks is most efficient in regions
23 of strong, high reaching convective activity such as the West Pacific (e.g., Aschmann et al.,
24 2009; Pisso et al., 2010; Marandino et al., 2013). The Asian monsoon represents another
25 important pathway to the lower stratosphere (e.g., Randel et al. 2010, Tissier and Legras, 2016)
26 entraining mostly Southeast Asian planetary boundary layer air with the potential to include
27 emissions from the Indian Ocean and Bay of Bengal (Fiehn et al., 2017, 2018b). In both regions,
28 the West Pacific and the Indian Ocean, these effective transport pathways may coincide with
29 strong oceanic emissions (e.g., Ziska et al., 2013) potentially leading to anomalously large
30 injection of brominated VSLS. While aircraft measurements in the West Pacific have confirmed
31 high concentrations of brominated VSLS such as CHBr_3 (Wales et al., 2018), the role of the
32 Asian monsoon as an entrainment mechanism for VSLS is not clear due to the lack of
33 observations in this region. Given the high variability of VSLS measurements in the tropical

1 tropopause layer (TTL) (Liang et al., 2010), the overall distribution and temporal short- and
2 long-term changes are not well known. Modelling the VSLS distribution in this region depends
3 on the magnitude and distribution of prescribed oceanic emissions, on the representation of
4 tracer transport in the models and on related uncertainties in both quantities (Hossaini et al.,
5 2016). Reconciling snapshots of VSLS distributions derived from high resolution aircraft
6 measurements with lower spatially and temporally smoothed global modelling fields remains a
7 challenge.

8 Changes in oceanic biogeochemical systems over the last decades most likely lead to changes in
9 the marine VSLS production. However, due to the sparse data coverage and missing process
10 understanding, it is currently not possible to quantify such long-term changes of the oceanic
11 halocarbon production and consequences for the air-sea flux (Ziska et al., 2017). Changes in
12 meteorological and oceanic surface parameters, which also impact the oceanic emission
13 strength, on the other hand, have been quantified. Based on increasing sea surface temperature,
14 salinity and wind speed, VSLS emissions are projected to increase over the recent past (Ziska
15 et al., 2013) and for future climate projections until 2100 (Tegtmeier et al., 2015, Ziska et al.,
16 2017). At the same time, atmospheric transport of VSLS is driven by changes of the
17 atmospheric circulation. In particular, changes of tropical, high reaching convection can be
18 expected to have a large influence on the transport of VSLS from the ocean surface to the TTL
19 (Aschmann et al., 2011; Hossaini et al., 2013). Long-term changes of VSLS injections into the
20 stratosphere are difficult to predict as they are driven by various processes including changes in
21 surface emissions, troposphere-stratosphere transport, and tropospheric chemistry (Pyle et al., 2007;
22 Hossaini et al., 2012a).

23 In our study, we combine observational data sets derived during upper TTL aircraft campaigns
24 with Lagrangian model simulations and an observation based VSLS emission climatology in
25 order to analyse the spatial and temporal variability of VSLS injection into the stratosphere.
26 Model simulations and data sets are introduced in Section 2. A detailed picture of the
27 distribution of CHBr₃ in the TTL (Section 3.1) is derived from Lagrangian transport simulations
28 applied to a bottom-up, observation-based emission inventory. Analyses of the trajectory
29 pathways and comparisons to aircraft observations allow us to evaluate how well we know the
30 hotspots of CHBr₃ injection (Sections 3.2 to 3.4). We will investigate if such hotspots are
31 mainly driven by oceanic or by atmospheric processes by analysing emission patterns and
32 transport pathways derived from the Lagrangian simulations. We present the first estimates of

1 the long-term changes of CHBr_3 injection based on changing oceanic emissions and transport
2 processes (Section 3.5). Finally, the overall contribution of CH_2Br_2 and CHBr_3 to the
3 stratospheric bromine loading is determined from the model simulations (Section 3.6) and
4 compared to existing studies. A summary and discussion of the key results is given in Section
5 4.

6

7 **2 Data and Model**

8 **2.1 Global emission climatology**

9 The global emission scenario from Ziska et al. (2013) is a bottom-up estimate of oceanic CHBr_3 ,
10 CH_2Br_2 , and CH_3I fluxes. Here we focus on the two brominated compounds. Static global
11 surface concentration maps of the two compounds were generated from atmospheric and
12 oceanic surface ship-borne in-situ measurements collected within the HalOcAt (Halocarbons in
13 the ocean and atmosphere) database project (<https://halocat.geomar.de>). In a first step, the in-
14 situ surface measurements were classified based on physical and biogeochemical characteristics
15 of the ocean and atmosphere important for the CH_2Br_2 and CHBr_3 distribution and sources. In
16 a second step, the global $1^\circ \times 1^\circ$ grid was filled by extrapolating the in-situ measurements within
17 each classified region based on the ordinary least square and robust fit regression techniques.
18 The method includes all in situ-measurements available through the HalOcAt data base at the
19 time, regardless of season and year of the measurement. The resulting concentration maps are
20 taken to represent climatological fields of a 23-year long time period covering 1979 to 2013.
21 Based on the global concentration maps the oceanic emissions were calculated with the transfer
22 coefficient parameterization of Nightingale et al. (2000), which was adapted to CHBr_3 and
23 CH_2Br_2 (Quack and Wallace, 2003). While the concentration maps do not provide any temporal
24 variability, the emission parameterization is based on 6 hourly meteorological ERA-Interim
25 data (Dee et al., 2011) allowing for relative emission peaks related to maxima in the horizontal
26 wind fields and sea surface temperature. The emission inventory is available at 6-hourly, daily,
27 and monthly temporal resolution or as a climatology product calculated as a long-term average
28 emission field. Seasonal CHBr_3 emission maps averaged over 1979-2013 are shown in the
29 supplementary material (Fig. S1).

1 2.2 Aircraft campaigns

2 We analyse the spatial and temporal variability of CHBr₃ in the TTL based on the comparison
 3 of Lagrangian transport simulations to data from aircraft campaigns. CHBr₃ measurements in
 4 the upper TTL are currently available from seven aircraft campaigns. Nearly all of the
 5 campaigns took place over Central America, except for the ATTREX campaign which was in
 6 large part conducted over the Pacific. Detailed information about the aircraft missions including
 7 location and time period are presented in Table 1.

8

9 **Table 1.** Aircraft campaigns with CHBr₃ measurements used in the study.

| Campaign (Aircraft) | Full name | Max. altitude | Location | Time period | Database/ Reference |
|--------------------------------|---|--------------------------|---|-------------------------------|---|
| ACCENT (WB-57) | Atmospheric Chemistry of Combustion Emissions Near the Tropopause | 19 km | Southern US Gulf of Mexico East Pacific | 1999 April, September | http://espoarchive.nasa.gov/archive/browse/accnt |
| Pre-AVE (WB-57) | Pre-Aura Validation Experiment | 19 km | Southern US Gulf of Mexico East Pacific | 2004 January – February | http://espoarchive.nasa.gov/archive/browse/pre_ave |
| AVE (WB-57) | Aura Validation Experiment | 19 km | Southern US Gulf of Mexico | 2005 June | https://espoarchive.nasa.gov/archive/browse/ave |
| CR-AVE (WB-57) | Aura Validation Experiment (Costa Rica) | 19 km | Southern US Gulf of Mexico East Pacific | 2006 January - February | https://espoarchive.nasa.gov/archive/browse/cr_ave |
| TC4 (WB-57) | Tropical Composition, Cloud and Climate Coupling | 19 km | Southern US Gulf of Mexico East Pacific | 2007 August | Toon et al. (2010) |

| | | | | | |
|--------------------------------|--|-------|-------------------------------|-----------------------------|---|
| SEAC4RS (ER-2) | Studies of Emissions, Atmospheric Composition, Clouds and Climate Coupling by Regional Surveys | 19 km | Southern US Gulf of Mexico | 2013 September | https://espo.nasa.gov/missions/seac4rs |
| ATTREX (Global Hawk) | Airborne Tropical TRopopause Experiment | 19 km | East Pacific | 2013 February - March | http://espo.nasa.gov/missions/attrex |
| | | 18 km | West Pacific | 2014 February - March | |

1

2 **2.3 VLSL transport modelling**

3

4 We are interested in the direct contribution of CHBr_3 and CH_2Br_2 to stratospheric halogen
5 loading in the form of source and product gas contributions. Therefore, the atmospheric
6 transport of the two compounds from the oceanic surface into the upper troposphere and TTL
7 is simulated with the FLEXPART Lagrangian particle dispersion model (Version 9.2 beta;
8 Stohl et al., 2005; 2010). The oceanic emissions, based on the sea-to-air flux data from Ziska
9 et al. (2013), prescribe the amount of CH_2Br_2 and CHBr_3 released in the FLEXPART
10 simulations with each air parcel trajectory. The global sea-to-air flux, given on a $1^\circ \times 1^\circ$ grid, is
11 used here at a monthly mean temporal resolution. For CHBr_3 , 90 trajectories are released per
12 month from each grid box carrying the gas amount prescribed by the emission scenario. For the
13 longer-lived CH_2Br_2 , 45 trajectories are released per month. Once all brominated SG and PG
14 has been removed from a trajectory through chemical decay and wet deposition, the trajectory
15 is automatically terminated, so that the number of all active trajectories stays roughly constant
16 (~ 20 million) at all times after the initial spin-up period. The global CHBr_3 simulations are run
17 for 35 years from 1979 to 2013 with a spin-up period of 6 months in order to analyse in detail
18 the spatial-temporal variability and long-term changes of stratospheric injection. For the longer-
19 lived CH_2Br_2 the spatial-temporal variability is known to be much smaller (Hossaini et al.,
20 2010) and runs are carried out for three years from 2011 to 2013 with a spin-up period of 18
21 months.

22 The transport in FLEXPART is driven by meteorological fields from the ECMWF (European
23 Centre for Medium-Range Weather Forecasts) reanalysis model. FLEXPART includes

1 parameterizations for moist convection (Forster et al., 2007) and turbulence in the boundary
2 layer and free troposphere (Stohl and Thomson, 1999), dry deposition, and scavenging (Stohl
3 et al., 2005). The runs are based on the 6-hourly fields of horizontal and vertical wind,
4 temperature, specific humidity, convective precipitation, and large scale precipitation from the
5 ECMWF reanalysis product ERA-Interim (Dee et al., 2011) given at a horizontal resolution of
6 $1^\circ \times 1^\circ$ on 60 model levels. A pre-processor retrieves the meteorological fields from the ECMWF
7 archive, including the vertical wind, which is calculated in hybrid coordinates mass-consistently
8 from spectral data. FLEXPART has been validated based on comparisons with measurement
9 data from three large-scale tracer experiments (Stohl et al., 1998) and with results from
10 intercontinental air pollution transport studies (e.g., Forster et al., 2001; Stohl and Trickl, 1999).
11 Previous FLEXPART studies using a similar model setup as applied here have shown a very
12 good agreement between diagnosed and observed VLSL profiles (e.g., Tegtmeier et al., 2013;
13 Fuhlbrügge et al., 2016).

14 FLEXPART includes the simulation of chemical decay by reducing the tracer mass carried by
15 each air parcel corresponding to its prescribed chemical lifetime. We set the atmospheric
16 lifetime of CHBr_3 (CH_2Br_2) to an altitude-dependent lifetime profile ranging from 16 (50) days
17 at the ocean surface to 29 (400) days in the TTL (Hossaini et al., 2012b). The lifetime profiles
18 were derived from simulations of the chemical tropospheric loss processes of CHBr_3 and
19 CH_2Br_2 with the chemical transport model TOMCAT (Chipperfield, 2006). Previously, profiles
20 from TOMCAT have been shown to agree well with aircraft observations in the tropical
21 troposphere (Hossaini et al., 2012b).

22 The bromine resulting from the photochemical loss of CH_2Br_2 and CHBr_3 , based on prescribed
23 loss terms, contributes to the inorganic product gases. In the FLEXPART simulations, these
24 product gases are grouped together as Br_y and transported together with the VLSL source gases
25 along the trajectory. Thus, we assume instantaneous conversion between organic intermediate
26 product gases and Br_y , which has been shown to be reasonable by Hossaini et al. (2010). Br_y
27 can be removed effectively from the troposphere through wet scavenging by rain or ice (Yang
28 et al., 2005). FLEXPART includes in-cloud as well as below-cloud scavenging, which is
29 initiated if the relative humidity as calculated from meteorological input data exceeds 80% and
30 the precipitation rate is larger than zero. In FLEXPART, the cloud scavenging ratio is used to
31 model washout of soluble species. The ratio is calculated within FLEXPART with the help of
32 the effective Henry's law coefficient, H_{eff} , which describes the physical solubility of a species

1 as well as the effects of dissociation. Among the members of the Br_y family, HBr and HOBr
2 can be washed out while the remaining species Br, BrO, BrONO₂, and Br₂ are not soluble. HBr
3 has a very large acidity dissociation constant resulting in an effective Henry's law coefficient
4 of 7.1×10^{13} M/atm for T = 298 K and pH = 5 (Yang et al., 2005). While HBr provides the main
5 pathway for wet removal of inorganic Br_y, HOBr is also soluble due to physical solubility, but
6 not due to dissociation (Frenzel et al., 1998) with $H_{\text{eff}} = 6.1 \times 10^3$ M/atm. In order to determine
7 which fractions of Br_y are in the form of HBr and HOBr, we apply the Br_y partitioning derived
8 from p-TOMCAT simulations (Yang et al., 2010).

9 Based on analysed wind-fields together with complex chemical schemes p-TOMCAT simulates
10 the tracer distribution in the troposphere and lower stratosphere including gaseous phase
11 bromine chemistry. The 3-dimensional Br_y field from p-TOMCAT and its partitioning into
12 HOBr, HBr, Br, BrO, BrONO₂, and Br₂ are given at a time step of 30 min. As the partitioning
13 of the Br_y field varies strongly with location and time, we apply it in a first step to every air
14 parcel according to its location each time before the wet deposition is initiated. In a second step,
15 wet deposition is calculated individually for each inorganic bromine species based on its
16 solubility specified by the effective Henry's law coefficient, as described above. Once wet
17 deposition is initiated the Br_y fraction determined to be washed out is removed completely.

18 Dissolved inorganic bromine can be released back to the gas phase by heterogeneous chemical
19 reactions (Abbatt, 2003; Salawitch, 2006), extending the tropospheric lifetime of Br_y by altering
20 the efficiency of wet deposition (von Glasow et al., 2004). The heterogeneous reactions on
21 aerosols which reactivate bromine radicals from the reservoir species (Yang et al., 2005; 2010)
22 are included in the chemical scheme of p-TOMCAT. This release of bromine back to the gas
23 phase results in elevated BrO/Br_y ratios (Yang et al., 2010) and thus a lower fraction of Br_y is
24 subject to wet deposition compared to a scenario without the heterogeneous chemical reactions.
25 As we directly use the p-TOMCAT Br_y partitioning for our trajectory simulations, these aerosol
26 effects have indirectly been taken into account when simulating the wet removal of Br_y.
27 Uncertainties in the modelled wet deposition arise from the parameterization of solubility via
28 the effective Henry's law coefficient and from uncertainties in the Br_y partitioning caused by
29 errors in the aerosols loading and in the mechanism used for heterogeneous reactions. Clouds
30 and aerosols within p-TOMCAT are not matched with those in FLEXPART which might lead to an
31 additional error source.

1 For the analysis of the spatial and temporal variability of CHBr_3 in the TTL from FLEXPART
2 simulations and aircraft observations in Sections 3.1 to 3.5, we use mixing ratios at 17 km
3 (approximate cold point) and mixing ratios averaged over 16-18 km (upper part of the TTL). In
4 order to derive the amount of VSLS source and product gases entrained into the stratosphere
5 from the model simulations in Section 3.6, we explicitly calculate the cold point along each
6 trajectory based on the ERA-Interim meteorological fields as stratospheric entrainment point.
7 The derived estimates of stratospheric VSLS entrainment depend on the meteorological input
8 data sets and on various FLEXPART model parameters, such as the convective
9 parameterization. The accurate representation of convection has been validated with tracer
10 experiments and ^{222}Rn measurements (Forster et al., 2007). The application of transport
11 timescales based on vertical heating rates instead of vertical wind fields in the TTL between 15
12 and 17 km results in only minor differences of VSLS entrainment (Tegtmeier et al., 2012).

13

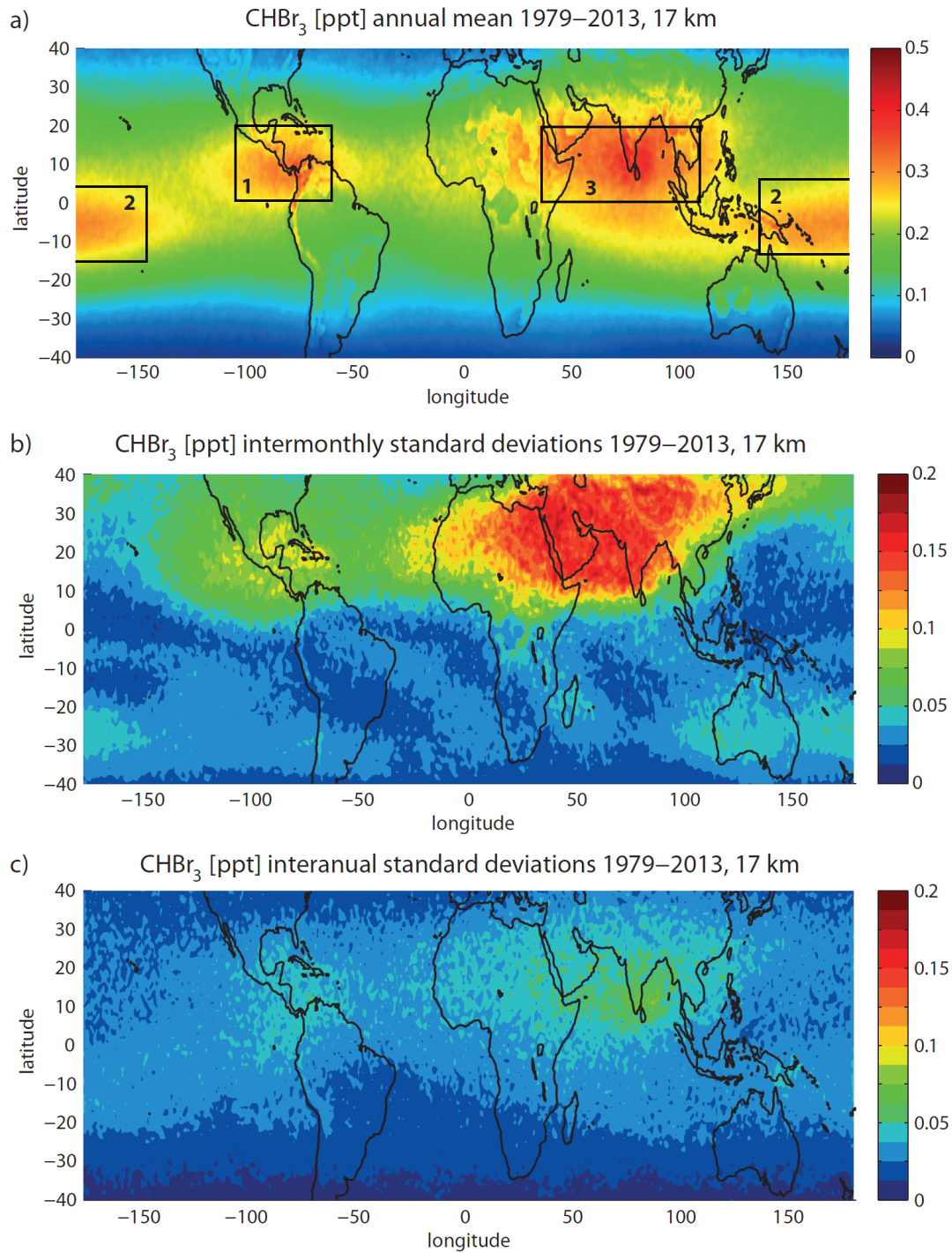
1 **3 Results**

3 **3.1 CHBr₃ in the TTL**

5 Figure 1a shows the long-term annual mean CHBr₃ distribution at 17 km as derived from the
6 Lagrangian transport calculations driven by monthly mean oceanic emission fields for the time
7 period 1979 – 2013. Clearly, CHBr₃ has a very pronounced spatial variability due to its short
8 lifetime. Largest CHBr₃ mixing ratios of up to 0.4 to 0.5 ppt can be found over 1) Central
9 America, 2) the Maritime Continent and tropical West Pacific and 3) tropical Indian Ocean (all
10 regions are highlighted by black squares in Figure 1a labelled from 1 to 3). Other tropical
11 regions with only little convective uplift show smaller mixing ratios, mostly between 0.1 and
12 0.2 ppt.

13 Entrainment of CHBr₃ into the stratosphere shows also a large temporal variability. The
14 seasonal variability is given here by the standard deviation over all monthly, multi-annual mean
15 values (Figure 1b). The by far most pronounced variability is found in the region of the Asian
16 Monsoon anticyclone, which is characterized by a strong seasonality of vertical transport
17 processes (Randel et al., 2010). Furthermore, the distribution of CHBr₃ at the cold point over
18 Central America shows some seasonal variations; however, of smaller magnitude. The
19 Maritime Continent and tropical West Pacific have only a very weak seasonal cycle. Overall,
20 the seasonal variations are more pronounced in the NH tropics and quite low in the SH tropics.
21 Seasonal CHBr₃ entrainment averaged over 1979-2013 are shown in the supplementary
22 material (Fig. S2).

24 Interannual variations are given in form of the standard deviation over all annual mean CHBr₃
25 mixing ratios at 17 km (Figure 1c). In comparison to the seasonal variability, the interannual
26 variability is relatively small in the NH tropics, but is of similar magnitude in the SH tropics.
27 Drivers of the seasonal and interannual variability will be discussed in the following sections.
28 We will analyse the three regions with maximum CHBr₃ entrainment identified above and
29 investigate the relative importance of emissions and transport processes for the overall
30 distribution and seasonality of stratospheric injection.



2

3

4 **Figure 1.** Modelled annual mean distribution of CHBr_3 at 17 km for 1979-2013 (a) and the inter-monthly
 5 (b) and inter-annual (c) variations given by the standard deviations over all monthly, multi-annual mean
 6 and annual mean values, respectively. Rectangles stand for regions of maximum CHBr_3 mixing ratios
 7 and will be discussed in detail in sections 3.2 to 3.4.

1 3.2 Central America

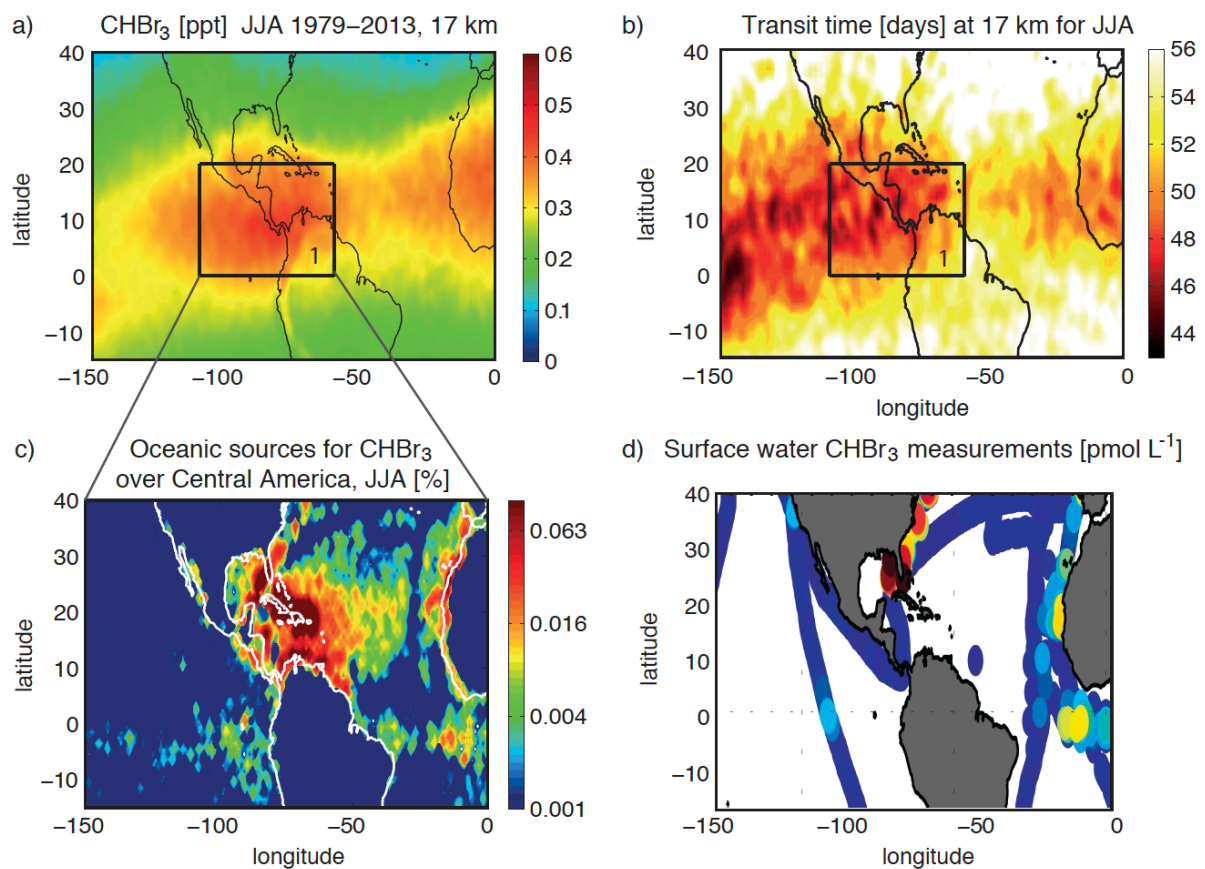
2

3 CHBr₃ in the TTL, on its way from the ocean surface to the stratosphere, shows a pronounced
4 maximum over Central America between 0°-20°N and 60°W-110°W (black square in Figures
5 1a and 2a). This maximum is present all year, but most pronounced during NH summer and
6 autumn. In the following, we will use the simulations for June/July/August to address the
7 question, if this maximum arises from very strong oceanic sources or from strong convective
8 transport. The impact of transport on the CHBr₃ distribution in the upper TTL is analysed by
9 estimating the time air masses need from the ocean surface to 17 km based on the FLEXPART
10 model simulations. The transport time of each trajectory is assigned to the location where the
11 trajectory reaches 17 km. A map of the ‘ocean surface – 17 km transit times’ is derived by
12 averaging over all trajectories on a 1°x1° grid. The tropical annual mean transit time is around
13 55 days with variations between 45 and 70 days (not shown here). Transit times over Central
14 America for the June/July/August season are relatively short with values around 48 days (Figure
15 2b). However, the transit times over the East and Central Pacific are similar or even shorter,
16 suggesting that the vertical transport in this region is as efficient as over Central America.
17 Therefore, atmospheric transport time scales alone cannot explain the CHBr₃ maximum over
18 Central America.

19 In addition to the transit time, we analyse the oceanic sources of CHBr₃ over Central America.
20 Each trajectory reaching the TTL over Central America (black square in Figure 2a) contributes
21 a certain amount of CHBr₃ to this local maximum by carrying it’s prescribed oceanic emission
22 (Ziska et al., 2013) from the surface to the cold point. The relative contribution (in %) of each
23 trajectory is assigned to its oceanic release point, thus quantifying which ocean region
24 contributes the largest amounts of CHBr₃ to the local maximum in the TTL. The relative
25 contributions averaged over 1°x1° grid cells (Figure 2c) demonstrate that the largest sources
26 stem from the Gulf of Mexico, the Caribbean Sea and the western North Atlantic. Some smaller
27 contributions come from the west coast of North Africa and from the equatorial Atlantic. The
28 co-occurrence of strong sources and the relatively short transport time scales over the Caribbean
29 Sea and Central America mainly cause the local CHBr₃ maximum in the Central American
30 TTL. While transport time scales are also short (or even shorter) in the eastern Pacific, oceanic
31 emissions are very small there and vice versa more pronounced emissions over the Atlantic and
32 along the coast of Africa do not cause a global maximum due to longer transport time scales.

1 The regional oceanic measurements in surface water, which were used to derive the
 2 extrapolated concentration and emission maps (Ziska et al., 2013), are given in Figure 2d. The
 3 available data show in particular high oceanic CHBr_3 concentrations at the Florida coastline
 4 and in the eastern part of the Gulf of Mexico. A reasonable amount of measurements with a
 5 distinctive distribution is available in this region supporting the extrapolated climatological
 6 source distribution, which leads to the CHBr_3 maximum in the TTL over Central America
 7 discussed above.

8



9

10 **Figure 2.** Modelled distribution of CHBr_3 at 17 km for JJA, 1979-2013 (a), transit time of air masses
 11 from the ocean surface to the TTL (b), oceanic source regions for CHBr_3 (c), and measurements of
 12 oceanic CHBr_3 concentrations from the HalOcat database used for Ziska et al. (2013) (d). The oceanic
 13 source regions in panel c are colour coded according to their contribution [% per $1^\circ \times 1^\circ$ grid box] to the
 14 amount of CHBr_3 at 17 km in the black box over Central America (highlighted in panels a and b).

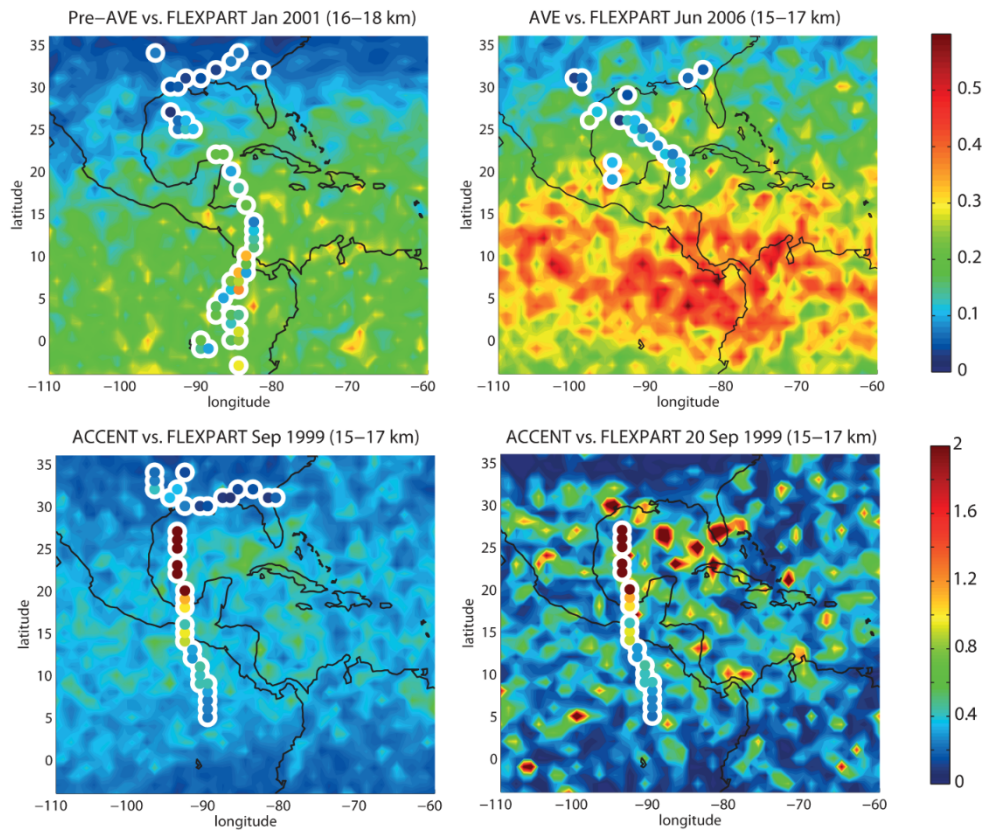
15

1 Over the last decades, the atmospheric distribution of CHBr_3 over Central America has been
2 investigated by a number of different aircraft campaigns. We will use available upper air
3 measurements to evaluate the distribution and variability of the model-derived CHBr_3 fields.
4 Details of the aircraft campaigns are given in Table 1. We show the spatial CHBr_3 distribution
5 in the TTL as observed during three different campaigns in comparison to the model simulations
6 (Figure 3). The altitude ranges in the upper TTL have been chosen so that each comparison
7 includes a maximum number of observational data. While for the aircraft campaigns individual
8 measurements are shown at the measurement locations, the model fields are averaged over the
9 duration of the respective campaign. This method allows us to evaluate the spatial distribution
10 of measured and modelled CHBr_3 fields, but it has the disadvantage of comparing in-situ data
11 with temporally averaged fields. We will discuss how this can impact the comparison and how
12 the temporal variability can be taken into account.

13 For the Pre-AVE campaign during Northern Hemisphere (NH) winter, CHBr_3 in the upper TTL
14 (16-18 km) shows a latitudinal gradient with small values of 0-0.1 ppt in the northern subtropics
15 and with higher values of up to 0.3-0.4 ppt around the equator. The same gradient is also evident
16 from the model simulation resulting in an overall good agreement. Similarly, for the AVE
17 campaign during NH summer, both, the observations and the model results, show a latitudinal
18 gradient with increasing values towards lower latitudes. However, here the overall agreement
19 is poor, since the model results are on average 50% larger than the measurements.

20

CHBr₃ [ppt], Aircraft campaign vs. FLEXPART



1

2 **Figure 3.** Modelled distribution of CHBr₃ in the upper TTL from FLEXPART (background colouring)
 3 in comparison with aircraft campaign measurements (coloured symbols with white edges). In the upper
 4 panels and lower left panel, all individual measurements from the respective campaign and the model
 5 mean over the same time period are shown. Only in the lower right panel, one individual flight
 6 (ACCENT flight from 20.09.1999) is shown with FLEXPART daily mean values to illustrate the large
 7 spatial variability including maximum values ≥ 2 ppt.

8

9 Finally, for the ACCENT campaign during NH autumn, the observations reveal extremely high
 10 CHBr₃ (up to 2 ppt) between 30°N and 20°N. While CHBr₃ is decreasing north and south of
 11 this area towards the range of 0.5-1 ppt, the values are still very high when compared to other
 12 campaigns over Central America. FLEXPART results, averaged over the time period of the
 13 ACCENT campaign (Sep 1999), show largest monthly mean CHBr₃ values of around 0.7 ppt,
 14 which are substantially smaller than the observations of 2 ppt. However, the model results look
 15 quite different and show large spatial inhomogeneities when evaluated at a daily mean
 16 resolution. Maximum model values are much higher for the daily resolution and in some
 17 locations, very close to the flight track, of similar size as the observations (around 2 ppt). The

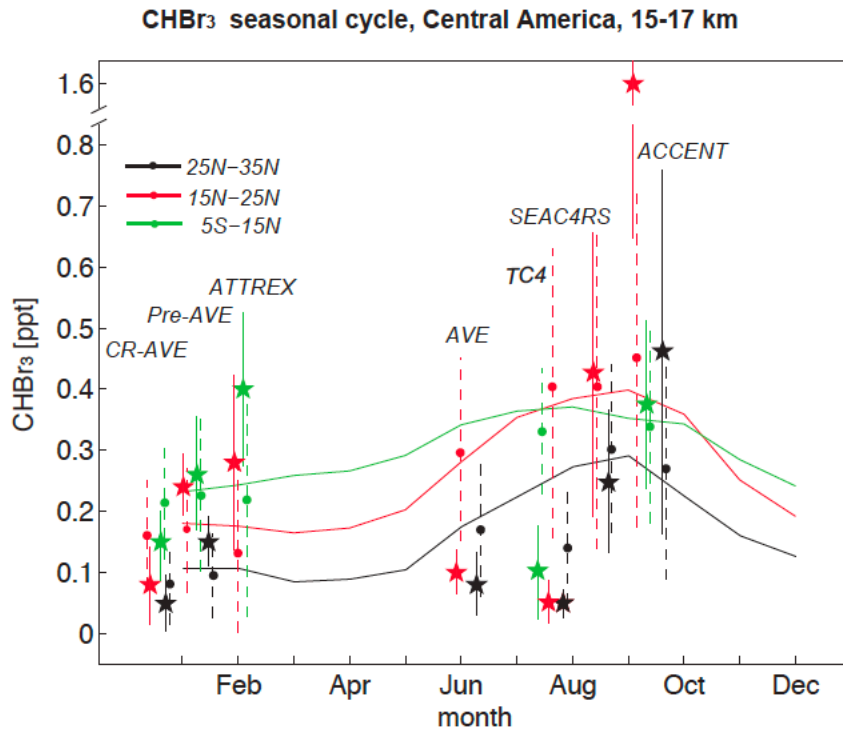
1 spotty features in the model simulations are a result of the high oceanic sources directly
2 underneath interacting with localized convective transport. The latter brings localized air
3 masses with very high CHBr_3 mixing ratios from the boundary layer into the 15-17 km layer.
4 The differences between monthly and daily mean model values make clear that CHBr_3 model-
5 measurement comparisons may be obscured by the high variability of the field. Given this high
6 variability and the existing uncertainties in the diagnosed oceanic sources and atmospheric
7 transport processes, it is very difficult for a model to predict the correct in-situ values at a given
8 time and measurement position. Nevertheless, if the large-scale emissions and transport fields
9 are correct, spatial and temporal averaging of the model results can be expected to produce
10 realistic mean VLS fields and to improve the agreement with observations. Only in cases
11 where rare events have been observed, averaging the CHBr_3 fields will not necessarily lead to
12 a better agreement with the measurements, as demonstrated above for the ACCENT campaign.
13 In consequence, it is important to include estimates of the spatial and temporal variability of
14 the CHBr_3 field in all comparisons.

15 A summary of the CHBr_3 model results compared to all aircraft campaigns in the Central
16 American region, taking into account spatial and temporal variability, is provided in Figure 4.
17 Here, we compare measurements averaged over different parts of the flight tracks (split by
18 latitude) with FLEXPART coincidences averaged over the same latitudinal bins. In addition,
19 the FLEXPART seasonal cycle averaged over 110°W - 80°W , the main longitudinal extent of
20 the aircraft campaigns, and the entire campaign time period (1999-2013), is shown. The
21 variability of the CHBr_3 distribution from observations and coincident model values is given
22 by the standard deviation over all values in the respective region. The comparison of the three
23 campaigns during NH winter shows an overall good agreement. For some latitude bins, the
24 modelled mean values agree very well with the observations (e.g., Pre-AVE for 5°S - 15°N),
25 for other regions, differences of the mean values can be up to 50-100%. However, all
26 observational mean values are within the standard deviations of the modelled field indicating
27 good agreement of model and measurements.

28

29

30



1

2 **Figure 4.** Seasonal cycle of CHBr₃ in the upper TTL (15-17 km) over Central America from
 3 FLEXPART simulations (solid lines) averaged over 110°W-80°W and 5°S-15°N (green), 15°N-25°N
 4 (red), and 25°N-35°N (black) for 1999-2013. In addition, aircraft measurements (stars) and coincident
 5 FLEXPART values (filled circles) are shown averaged over the same latitude bins and corresponding
 6 to the respective year of the campaign. Temporal and spatial variability of average measurements (solid
 7 vertical lines) and coincident model values (dashed vertical lines) is shown in form of the 1-sigma
 8 standard deviations over all values in the respective bin.

9

10 For the campaigns during NH summer, mean differences are in general larger than during NH
 11 winter. At the same time, the temporal and spatial variability of the simulated and observed
 12 CHBr₃ distribution is also larger so that most observations agree with the coincident model
 13 values within their uncertainties. The large differences between the individual campaigns
 14 during NH summer confirm the increased variability suggested by the model results. For two
 15 of the campaigns (AVE and TC4), FLEXPART overestimates the CHBr₃ values during this
 16 time of the year, while for the other two campaigns (SEAC4RS and ACCENT), the observations
 17 and modelled values agree relatively well except for one outlier. Particularly high CHBr₃ exists
 18 for the 15°N-25°N region, observed during the ACCENT campaign at the top altitude of a
 19 plume extending from 14 – 16 km near Houston, Texas. This value is larger than the model
 20 mean, although observational and model uncertainties slightly overlap. In total, observations

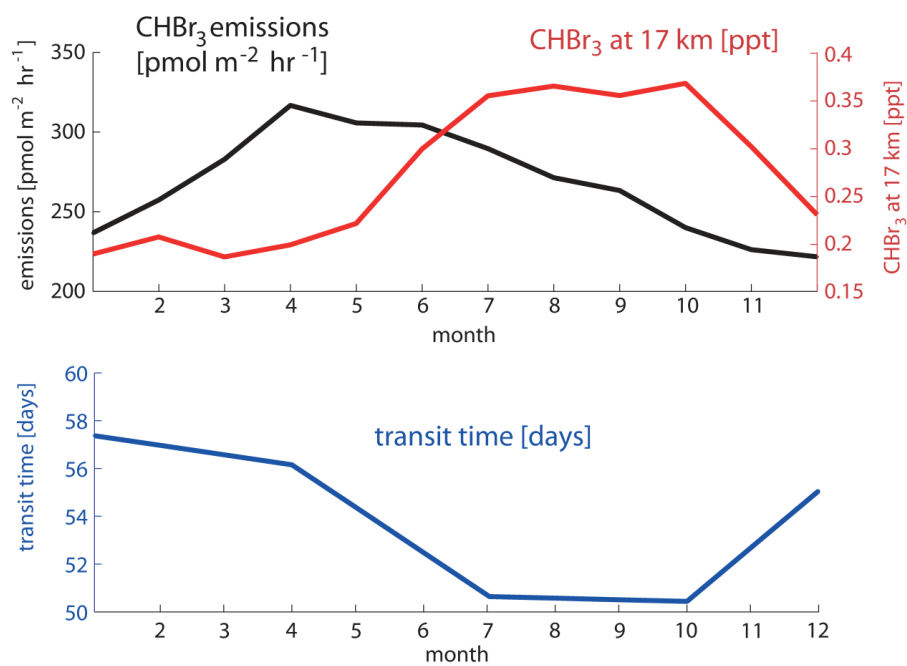
1 and model agree reasonably well with a larger variability during the NH summer and early
2 autumn period. For this time of the year, the model also suggests a seasonal CHBr₃ maximum
3 which is confirmed by measurements from SEAC4RS and ACCENT, but not by the AVE and
4 TC4 campaigns.

5

6 CHBr₃ in the upper TTL over Central America shows pronounced seasonal variations as
7 revealed by the comparisons to aircraft campaigns in Figure 4. The CHBr₃ seasonal cycle at 17
8 km shows a maximum from July to October (~0.37 ppt) and a minimum from January to April
9 (~0.17 ppt) (Figure 5a). Such seasonal variations can be caused by variations of the oceanic
10 emissions or the atmospheric transport times. First, we analyse the seasonal cycle of CHBr₃
11 emissions, averaged over the source region identified earlier, which show peak emissions from
12 April to June of up to 320 pmol m⁻² hr⁻¹. This peak in surface emissions in late spring/early
13 summer is consistent with a peak in the TTL around 2 months later, as the mean transit time
14 from the surface to 17 km in this region is about 55 days. Second, we analyse the seasonal cycle
15 of the transit time and find a minimum from July to October, which is also consistent with the
16 highest CHBr₃ values in the TTL during the same time period. While the amplitude of the
17 seasonal cycle in CHBr₃ in the TTL is around 74%, seasonal variation of the emissions and the
18 transit time are only 36% and 15%, respectively. However, the amplitude in transit time does
19 not directly translate into the amplitude in CHBr₃ in the TTL, given the logarithmic nature of
20 the atmospheric lifetime of chemical compounds. Overall, the interaction of both processes,
21 oceanic emissions and transit time, cause the pronounced seasonal cycle of CHBr₃ over Central
22 America.

23

24

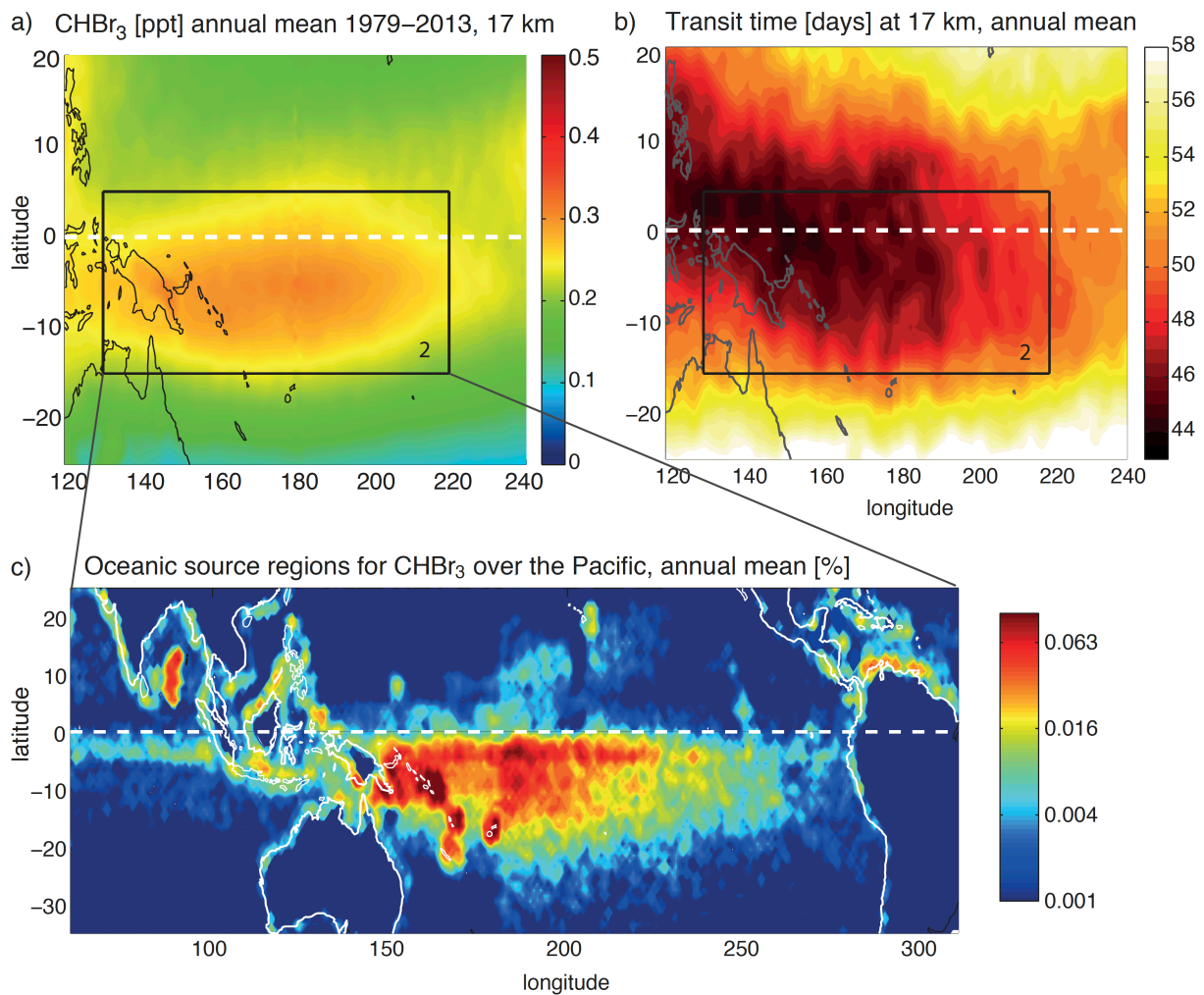


1
 2 **Figure 5.** Seasonal cycle of CHBr₃ at 17 km over Central America (black square in Figure 2a) from
 3 FLEXPART simulations (red line), of oceanic CHBr₃ emissions averaged over the respective source
 4 region (black line) and of the 'surface – 17 km' mean transit time (blue line) are shown.

3.3 Maritime Continent and tropical West Pacific

CHBr₃ in the TTL shows a pronounced maximum over the Maritime Continent and tropical West Pacific between 15°S-5°N and 130°E-220°E (black square in Figures 1a and 6a). An important characteristic of this CHBr₃ maximum (referred to as the West Pacific maximum hereinafter) is that the high values are not distributed symmetrically across the equator but are shifted southwards. The maximum is present all year with no pronounced seasonal cycle (see Figure 1b). In the following, we will use annual mean results to investigate if the high values arise from very strong oceanic sources or from strong convective transport. The transit time shows smallest values of around 45 days in the West Pacific and over the Maritime continent (Figure 6b). The most important deviation from the CHBr₃ distribution at 17 km is that over the West Pacific the shortest time scales and thus most efficient transport are not centred in the Southern Hemisphere, but they are distributed symmetrically across the equator.

Oceanic sources for CHBr₃ in the West Pacific upper TTL (black square in Figure 6a) stem mostly from the Pacific Ocean, the Maritime Continent and also to a smaller degree from Central America (Figure 6c). The trajectory analysis clearly shows that the largest contribution comes from the West Pacific south of the equator, while the oceanic contributions north of the equator are lower. This pattern is directly related to the emission inventory used in this study (Ziska et al., 2013), which suggests overall stronger emissions in the southern Pacific Ocean (see Figure S1 in the supplementary material). However, available open ocean surface measurements in both, NH and SH Pacific Ocean, were sparse during the time of the construction of the inventory and mostly based on the TransBrom Sonne campaign (Krüger and Quack, 2013). The latitudinal gradient of the emission inventory with stronger emissions in the SH is based on the in-situ measurements along one cruise track from Japan to Australia during October 2009 and may not be representative for other seasons and other West Pacific regions. Future ship campaigns are necessary to confirm or improve the existing emission inventory.



1

2 **Figure 6.** Modelled distribution of CHBr₃ at 17 km, annual mean 1979-2013 (a), transit time of air
 3 masses from the ocean surface to the TTL (b), and oceanic source regions for CHBr₃ at 17 km (c).
 4 Oceanic source regions are colour coded according to their contribution [% per 1°x1° grid box] to the
 5 amount of CHBr₃ at 17km in the black box over the West Pacific (highlighted in panels a and b).

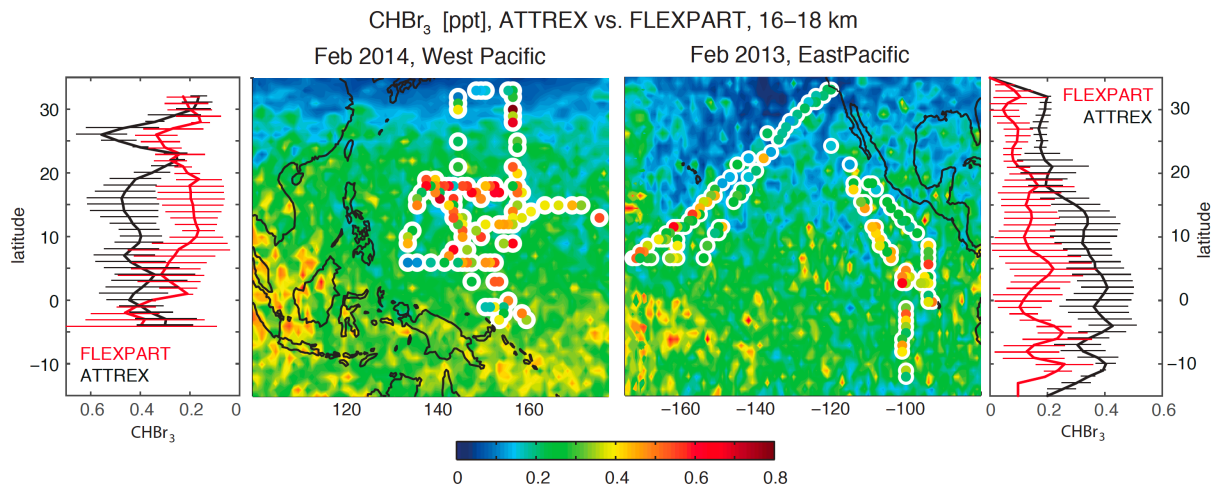
6

7

8 Pacific aircraft campaigns are used to further analyse the hemispheric differences of the
 9 diagnosed CHBr₃ distribution. ATTREX measurements in the West Pacific in 2014 and in the
 10 East Pacific in 2013 are compared to FLEXPART simulations in Figure 7. In both regions, the
 11 comparison reveals a reasonably good agreement with increasing CHBr₃ values towards lower
 12 latitudes. In the West Pacific, measurements and coincident model values agree best south of
 13 10°N, while north of this the model underestimates observations by up to 0.3 ppt. In the East
 14 Pacific, model values and measurements are closer in the NH and agree mostly within their

1 error bars. South of the equator, however, measurements are constantly larger with differences
 2 of up to 0.3 ppt. In total the modelled CHBr₃ entrainment over the Pacific is too small when
 3 compared to measurements, which could be due to an underestimation of the oceanic emissions
 4 in this region.

5



6

7 **Figure 7.** Modelled distribution of CHBr₃ in the uppermost TTL from FLEXPART (background
 8 colouring) in comparison with ATTREX aircraft campaign measurements (coloured symbols with white
 9 edges). Zonal means of coincident model-measurement comparisons are given in the leftmost panel for
 10 FLEXPART and the ATTREX campaign in February/March 2014 in the West Pacific and in the
 11 rightmost panel for FLEXPART and the ATTREX campaign in February/March 2013 in the East
 12 Pacific. Temporal and spatial variability of measurements and coincident model values is shown in form
 13 of the 1-sigma standard deviations over all values in the respective zonal bin (horizontal lines).

1 3.4 Tropical Indian Ocean

2

3 Annual mean CHBr_3 in the uppermost TTL shows a pronounced maximum over India, the Bay
4 of Bengal and the Arabian Sea between 2°N - 22°N and 35°E - 110°E (Figures 1a, referred to as
5 the Indian Ocean maximum hereinafter). The simulations diagnose in the long-term mean, the
6 globally highest TTL CHBr_3 values of up to 0.5 ppt over the southern tip of India. At the same
7 time, the intermonthly standard deviation is very high over this region (Figure 1b) due to
8 pronounced seasonal variations. During NH summer (June/July/August), high CHBr_3 values of
9 around 0.6 ppt are found over a large region stretching from South-East Asia all the way to
10 North-East Africa between 10°N and 25°N . During SH summer (December/January/February),
11 smaller maximum values of around 0.4 ppt CHBr_3 are diagnosed south of India over the Indian
12 Ocean between 5°S - 10°N (Figure 8).

13 In order to evaluate the transport efficiency for oceanic short-lived trace gases in this region,
14 the transit time is calculated from the trajectory analysis for the NH and SH summer seasons.
15 During NH winter, transit times from the surface to the TTL show a very similar pattern as
16 CHBr_3 in the TTL, with shortest transit times of around 45 days over the Indian Ocean
17 coinciding with largest CHBr_3 abundance. During NH summer, on the other hand, the transit
18 times minimize not in the region of maximum CHBr_3 abundance, but instead south of this
19 region where air masses can reach the TTL within 43 days. Between 10°N and 25°N , the
20 transport is still fast and the transit of short-lived species from their ocean sources will take
21 around 48 days. Overall the transit time is similar to values found for the West Pacific and
22 cannot solely account for the simulated maximum CHBr_3 values.

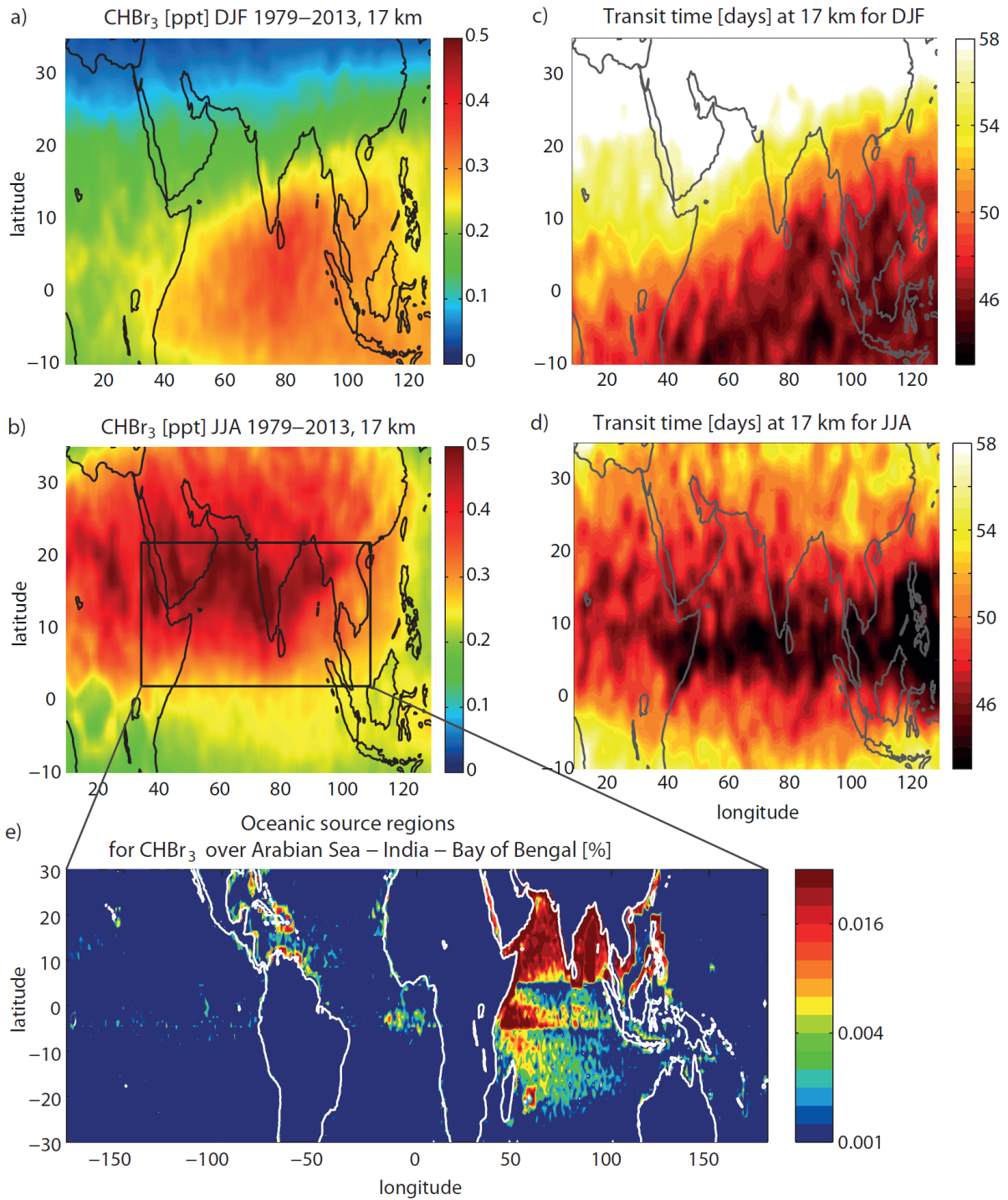
23 CHBr_3 contributing to the Indian Ocean TTL maximum mostly stems from the Bay of Bengal,
24 the Arabian Sea, the equatorial region of the Indian Ocean and the coast lines of South-East
25 Asian countries like China. Compared to the oceanic contributions identified for the Central
26 America and West Pacific maxima, sources for the Indian Ocean CHBr_3 maxima show a large
27 regional extent including coastal and open ocean emissions from 20°S to 30°N . Given that
28 oceanic emissions from large parts of the Indian Ocean and adjacent coastal areas can be
29 transported into the Asian monsoon region (Fiehn et al., 2017), the CHBr_3 maxima can be
30 explained by the strong oceanic emissions in this region combined with efficient boundary layer
31 –TTL transport.

1 The global maximum of CHBr_3 over India, Bay of Bengal and the Arabian Sea is also subject
2 to the largest uncertainties when compared to the other maxima found in our model simulations.
3 For the construction of the emission inventory from Ziska et al. (2013), only one data set was
4 available for the Indian Ocean (Yamamoto et al., 2001). The data set is based on measurements
5 at seven stations in the open ocean waters of the Bay of Bengal and reveals relatively high
6 CHBr_3 values between 8 and 15 ng/L. Given the great distance of the sampling points from the
7 coasts, the authors hypothesized that planktonic production is the most probable source for this
8 high CHBr_3 abundance. Independent measurements from the OASIS campaign in 2014 confirm
9 the subtropical and tropical West Indian Ocean as a strong source for CHBr_3 to the atmosphere,
10 although open ocean surface concentrations were overall lower with maximum values of 8 ng/L
11 (Fiehn et al., 2017). A recent update of the Ziska bottom-up CHBr_3 emission climatology (Fiehn
12 et al., 2018b) suggests enhanced emissions in the tropical Indian Ocean, which would lead to
13 even higher stratospheric entrainment in this region. While the high values from Yamamoto et
14 al. (2001) were used locally for the emission climatology, the rest of the tropical Indian Ocean
15 was filled by applying open ocean data from the tropical Atlantic and Pacific. In consequence,
16 the emission scenario for the Indian Ocean has large uncertainties and further VLSL
17 measurements are required to confirm or improve our estimates of the Indian Ocean as the
18 region of strongest CHBr_3 entrainment into the stratosphere.

19

20

21



1

2

3 **Figure 8.** Modelled distribution of CHBr_3 at 17 km for DJF and JJA 1979-2013 (a, b). Transit time of
 4 air masses from the ocean surface to the TTL for DJF and JJA (c, d). Oceanic source regions colour
 5 coded according to their contribution to CHBr_3 at 17km over Arabian Sea, India and Bay of Bengal
 6 (black box in panel b) given in % per $1^\circ \times 1^\circ$ grid box (e).

1 3.5 Interannual and long term changes

2 Long term changes of tropical mean (30°N-30°S) CHBr₃ mixing ratios at 17 km show a weak
3 but significant trend of 0.017 ± 0.012 ppt Br/decade, corresponding to a 10% increase of CHBr₃
4 over the whole time period (1979-2013). Regionally, the long term changes are more
5 pronounced and FLEXPART simulations suggest decreasing or increasing CHBr₃ in the TTL
6 depending on the location (Figure 9). Over South America, Australia and the Central/East
7 Pacific, the trend is not significant given the relatively small trend values compared to the
8 interannual variability found here. For all other regions, CHBr₃ shows a significant, positive
9 trend of 2-10% per decade. CHBr₃ over the Indian Ocean and Maritime Continent is highlighted
10 in Figure 9c as the region with the maximum trend (0.04 ppt Br/decade), mostly driven by the
11 ENSO-related steep changes over the time period 2000-2013 (Fiehn et al., 2018a). CHBr₃ over
12 the East Pacific is highlighted in Figure 9b as an example of a negative, but not significant trend
13 (-0.017 ppt Br/decade).

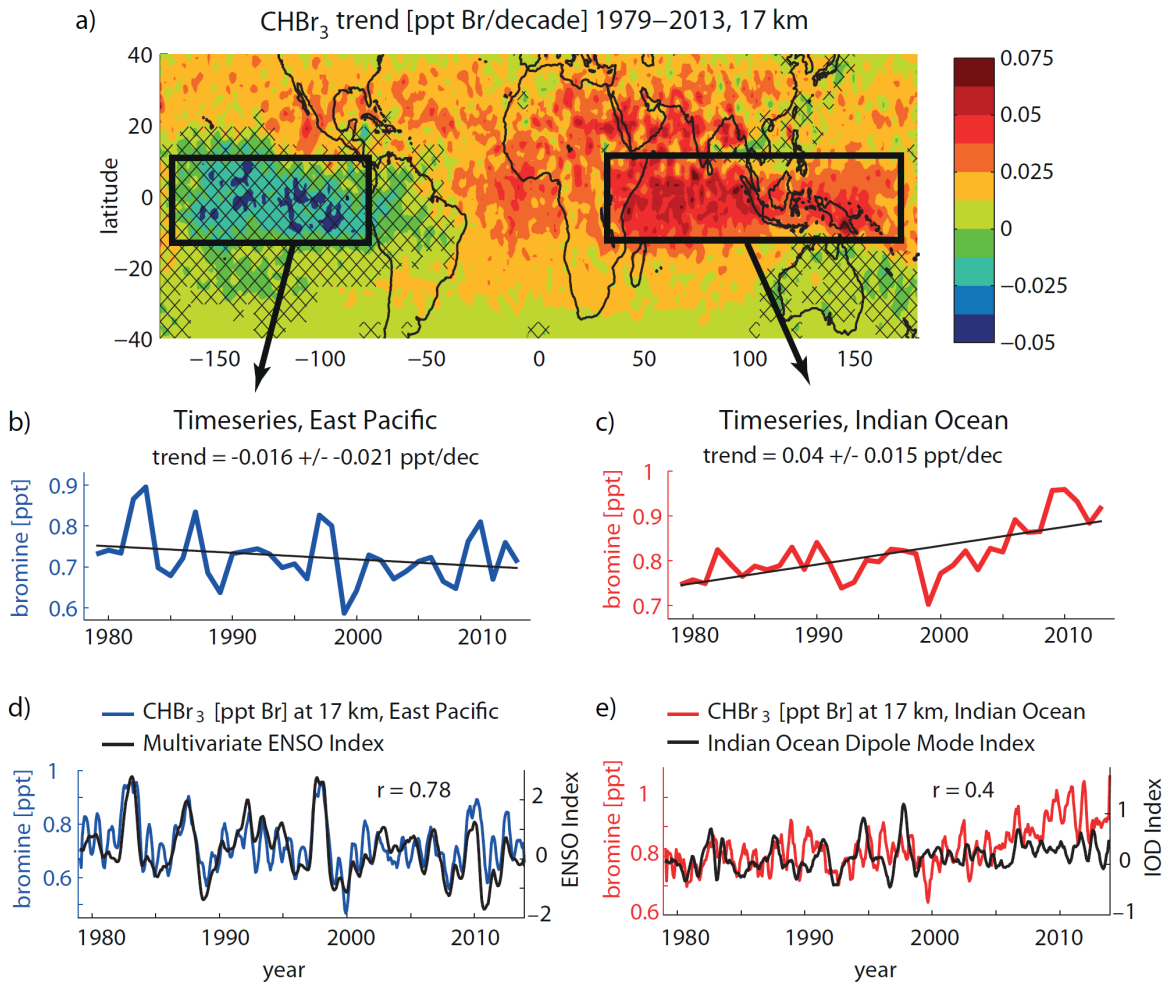
14 The projected interannual and long-term changes of CHBr₃ injections are driven by the
15 variability of oceanic emissions (Ziska et al., 2013), convective transport from the surface to
16 the TTL (Aschmann et al., 2011) and transport in the TTL (Krüger et al., 2009). Our model
17 runs are based on CHBr₃ emissions that allow for changes over time due to changing
18 meteorological surface parameters (mostly ERA-Interim), but do not take into account oceanic
19 biogeochemical and related CHBr₃ production changes. Due to increasing sea surface
20 temperature and wind speed, CHBr₃ emissions increase considerably by 7.9% from 1979 to
21 2013 (Ziska et al., 2017). Changes in the modelled atmospheric transport are driven by long-
22 term changes in ERA-Interim parameters such as temperature, winds and humidity fields
23 leading to an overall trend of CHBr₃ at 17 km of 10% for 1979-2013.

24 The two CHBr₃ time series over the East Pacific and Indian Ocean/Maritime Continent (Figure
25 9b and 9c) show the opposite long-term behaviour, but also share some of the same patterns of
26 interannual variability. In particular, signals like the steep CHBr₃ decrease from 1997/1998 to
27 1999, the increase from 2008 to 2009/2010 and the relatively high values in 1982 are common
28 to both time series. We analyse the common and separate drivers of the variability of the two
29 time series further by comparing them to modes of tropical climate variability.

30 First, we compare the time series of stratospheric bromine in the East Pacific with the
31 Multivariate ENSO Index (MEI; Wolter and Timlin, 2011) in Figure 9d. The irregular ENSO
32 variations in winds and sea surface temperatures over the tropical eastern Pacific Ocean drive

1 changes in CHBr_3 emissions and atmospheric transport leading to a high correlation of the two
 2 time series ($r = 0.78$). During El Niño years, water in the central and eastern Pacific becomes
 3 warmer than usual and the dry and steady easterly winds turn into warm and moist westerlies
 4 leading to an increase of the oceanic emissions. This increase is driven by meteorological and
 5 oceanic surface variations but does not allow for possible changes in biogenic CHBr_3
 6 production related to changes in the eastern Pacific upwelling system (Hepach et al., 2016). At
 7 the same time the warm East Pacific favours stronger convection intensifying the VLSL
 8 transport into the TTL (Aschmann et al., 2011). Overall, El Niño years lead to enhanced CHBr_3
 9 injection over the East Pacific (e.g., 1982, 1986, 1991, and 1997), while La Nina corresponds
 10 to weaker CHBr_3 injection (e.g., 1988, and 2010).

11



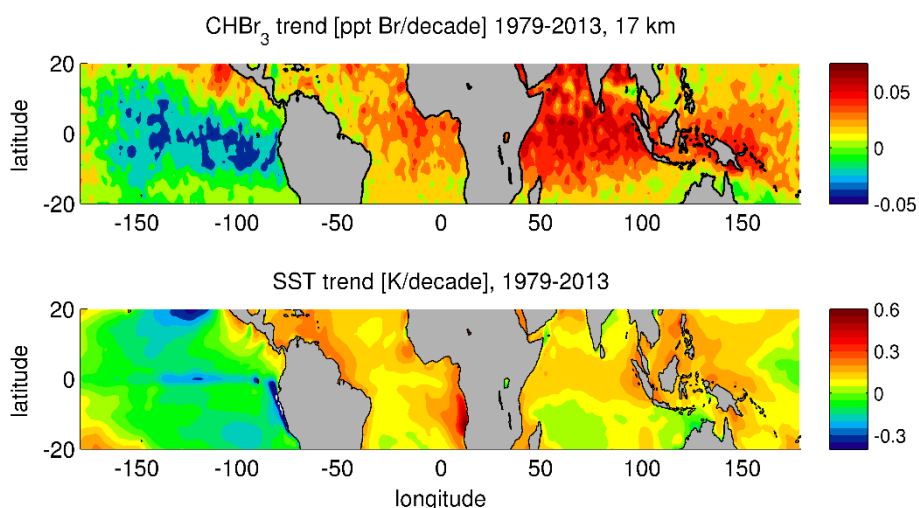
12

13

1 **Figure 9.** Modelled long-term change of CHBr₃ [Br/decade] at 17 km for the time period 1979-2013
2 (a). Time series (annual means) averaged over the East Pacific and the Indian Ocean/Maritime
3 Continent/West Pacific region are shown together with the trend (b, c). Time series (5 months running
4 mean) are shown together with the ENSO index and Indian Ocean Dipole index, respectively (d, e).

5
6 Second, variations of CHBr₃ at 17 km over the Indian Ocean and Maritime Continent are shown
7 together with the Indian Ocean Dipole (IOD) Mode Index (Figure 9e), an indicator of the east-
8 west temperature gradient across the tropical Indian Ocean (Saji et al., 1999). The two
9 timeseries are weakly correlated ($r=0.4$) sharing some of their variability. The IOD is a coupled
10 ocean-atmosphere phenomenon with anomalous cooling of the south eastern tropical Indian
11 Ocean and anomalous warming of the western tropical Indian Ocean during a positive phase.
12 Associated with these changes the convection normally situated over the eastern Indian Ocean
13 warm pool shifts to the west. For some years, the positive phase results in slightly stronger
14 CHBr₃ emissions and more effective atmospheric transport (e.g., 1982-83, 2006). In other years,
15 strong IOD events will not impact the CHBr₃ abundance over the Indian Ocean/Maritime
16 Continent (e.g., 1997-98). The relatively weak correlation of CHBr₃ injection and IOD results
17 from the influence of the ENSO signal on atmospheric transport in this region. A combination
18 of SST anomalies in the West Indian Ocean and the ENSO signal can have varying impacts on
19 the CHBr₃ injection depending on the time of year (Fiehn et al., 2018a). While positive SST
20 anomalies together with El Niño conditions in boreal winter and spring enhance stratospheric
21 VSLs injection, La Niña conditions in boreal fall can also cause stronger than normal
22 stratospheric injection. Overall, the inter-annual variability of the CHBr₃ time series is driven
23 by a combination of the ocean-atmosphere modes in the Indian and Pacific Ocean, however,
24 the strong increase during 2009-2013 is not related to either of the two modes.

25



1
 2 **Figure 10.** Modelled long-term change of FLEXPART CHBr₃ [ppt Br/decade] at 17 km and ERA-
 3 Interim sea surface temperature (SST) [K/decade] for the time period 1979-2013.

4
 5 The overall pattern of long-term CHBr₃ changes at 17 km shows a strong similarity to the long-
 6 term changes in sea surface temperature derived from ERA-Interim data (Figure 10). While the
 7 global mean surface temperature has increased due to anthropogenic greenhouse gas emissions
 8 (Hegerl et al., 2007), the spatial pattern of global warming is more complex. Most regions
 9 exhibit a warming trend over the 35 year period, however, much of the eastern Pacific cooled.
 10 This cooling may either be related to an unusual strong manifestation of internal variability in
 11 the observations or may be caused by external, regional forcings (e.g., Wang et al., 2012; Luo
 12 et al., 2012). ERA-Interim long-term temperature changes over the tropical oceans show good
 13 agreement with HadCRUT, a combined dataset of instrumental temperature records, with only
 14 small differences (Simmons et al., 2014). Most interesting for our analysis is the correlation
 15 between the SST trends and the long-term changes of stratospheric CHBr₃ entrainment. Regions
 16 with large positive SST trends such as the Indian Ocean, East Atlantic and Maritime Continent
 17 coincide with regions where the CHBr₃ entrainment trend is strongest. The east Pacific, on the
 18 other hand, stands out as the region where the SST cooling trend coincides with decreasing
 19 CHBr₃ entrainment. While this relation holds for many oceanic regions, we also find outliers
 20 such as the southern Indian Ocean, where SST trends are around zero but CHBr₃ entrainment
 21 shows a strong positive trend. Based on our modelling approach, the interaction of two
 22 mechanisms causes the strong correlation between the SST and CHBr₃ trends. Higher sea
 23 surface temperatures and stronger surface winds force a larger flux of CHBr₃ out of the ocean

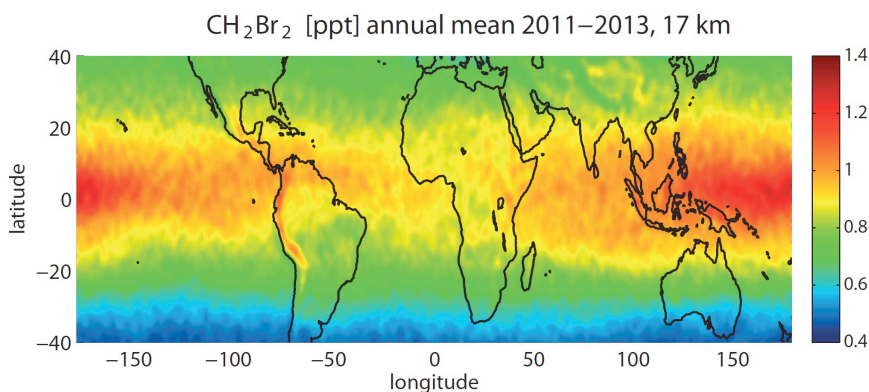
1 into the atmosphere (Ziska et al., 2013) and at the same time cause enhanced convection,
2 transporting surface air masses into the TTL (Tegtmeier et al., 2015). As the cold point
3 tropopause altitude shows no significant trend in radiosondes or ERA-Interim data over the
4 1980-2013 time period (Tegtmeier et al., 2020), CHBr₃ changes at 17 km correspond directly to
5 changes of stratospheric CHBr₃ entrainment. Future SST changes can be expected to drive a
6 continued positive trend of stratospheric CHBr₃ entrainment (Hossaini et al., 2012a).

1 3.6 Overall CH₂Br₂ and CHBr₃ contribution to stratospheric bromine

2

3 CHBr₃ together with CH₂Br₂ provides the main contribution of oceanic bromine to the
4 stratosphere. CH₂Br₂ mixing ratios in the inner tropical belt (10°S-10°N) show less variability
5 than CHBr₃, consistent with the longer lifetime, and range between 0.9 and 1.4 ppt. Largest
6 values can be detected over the West and Central Pacific and are distributed evenly over both
7 hemispheres (Figure 11). There is no local CH₂Br₂ maxima over the Indian Ocean, as observed
8 for CHBr₃, since no strong localized sources in the region exist according to the Ziska et al.,
9 (2013) climatology. However, new ship measurements in the western Indian Ocean revealed
10 high CH₂Br₂ surface water concentrations, i.e., south of Madagascar in July 2011 (Fiehn et al.,
11 2017). Seasonal and interannual variations of CH₂Br₂ are much weaker than for CHBr₃ resulting
12 in a continuous bromine entrainment into the stratosphere.

13



14

15 **Figure 11.** Modelled tropical annual mean distribution of CH₂Br₂ [ppt] at 17 km for 2011-2013.

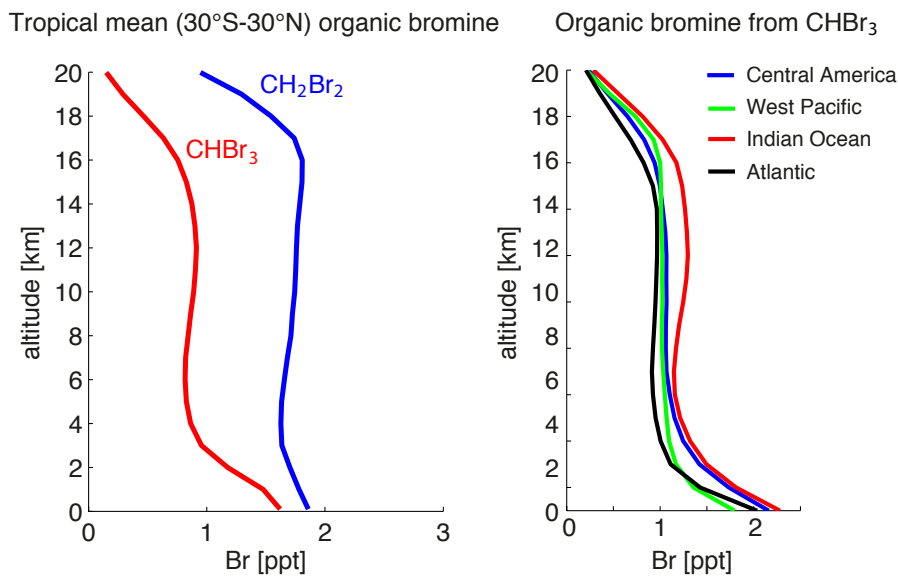
16

17 Figure 12 shows the annual, tropical mean CHBr₃ and CH₂Br₂ profiles averaged over 1979-
18 2013. At the surface, tropical mean values of 1 ppt CH₂Br₂ and 0.6 ppt CHBr₃ are simulated,
19 which are slightly smaller than reported observations (Ziska et al., 2013 and references therein).
20 Mixing ratios in the free troposphere decrease by nearly 50% (10%) for CHBr₃ (CH₂Br₂) when
21 compared to the marine boundary layer. Both gases are well mixed in the free troposphere with
22 nearly constant mixing ratios of 0.3 and 0.9 ppt for CHBr₃ and CH₂Br₂, respectively,
23 corresponding to 0.9 ppt and 1.8 ppt bromine (Figure 12). CHBr₃ shows a slight S-shape with
24 elevated abundances around 12-14 km related to strong convective outflow at this level bringing

1 marine boundary layer air directly into the lower TTL. Above 14 km, CHBr₃ mixing ratios start
2 to decrease reaching values of 0.22 ppt at 17 km close to the cold point, corresponding to 0.66
3 ppt bromine. CH₂Br₂ mixing ratios, on the other hand, stay nearly constant up to 18 km, as
4 expected based on its quite long lifetime of 400 to 500 days in the TTL, reaching values of 0.9
5 ppt (1.8 ppt bromine).

6 CHBr₃ profiles for four different regions (Figure 12) show that surface atmospheric mixing
7 ratios are strongest in the Indian Ocean and Central America. Overall maximum mixing ratios
8 over the Indian Ocean result from strong surface emissions combined with a relatively strong
9 transport and main convective outflow between 11 and 14 km giving an S-shape CHBr₃ profile.
10 Only for the West Pacific, transport into the stratosphere is more efficient, however, smaller
11 emissions lead to the total entrainment over this region being smaller than over the Indian
12 Ocean.

13



14

15 **Figure 12.** Modelled vertical profiles of CHBr₃ and CH₂Br₂ [ppt Br] in the tropics (30°S-30°N) (left
16 panel) and of CHBr₃ for Central America (0°-20°N, 70°W-110°W), West Pacific (15°S-5°N, 140°E-
17 150°W), Indian Ocean (0°-20°N, 40°E-110°E), and Atlantic (0°-20°N, 20°W-50°W) (right panel) for
18 1979-2013.

19

20 Table 2 gives the contribution of CHBr₃ and CH₂Br₂ to the stratospheric bromine loading based
21 on source gas (SG) injection alone and based on the sum of source and product gas (PG)

1 injection. CHBr_3 and CH_2Br_2 have been evaluated directly at the cold point (as given by ERA-
 2 Interim) and contribute 2.4 ppt Br to stratospheric bromine loading directly in form of SG
 3 entrainment with 75% (25%) resulting from CH_2Br_2 (CHBr_3). The CHBr_3 estimates of 0.2 ppt
 4 (corresponding to 0.6 ppt Br) are in agreement with other studies which range from 0.1 ppt
 5 (Warwick et al., 2006; Aschmann et al., 2009) to 0.35 ppt (Hossaini et al., 2012b). For CH_2Br_2 ,
 6 our results of 0.9 ppt (corresponding to 1.8 ppt Br) agree very well with CTM modelling studies
 7 (Hossaini et al., 2012b) which give estimates of 0.75 – 0.9 ppt. The overall contribution of the
 8 two gases in form of SG and PG entrainment of 4.7 ppt is also in good agreement with earlier
 9 studies giving estimates ranging from 4-5 ppt (Hossaini et al., 2013) to 7.7 ppt (Liang et al.,
 10 2014).

11

12 **Table 2.** Modelled contribution of CHBr_3 and CH_2Br_2 to the stratospheric halogen loading in form of
 13 source gas (SG) and total (SG+PG) contribution for 2011-2013.

| Br [ppt] | Inner tropics (10°S-10°N) | | Tropics (30°S-30°N) | |
|--|---------------------------|-------------------|---------------------|-------------------|
| | PG [ppt Br] | PG+SG [ppt Br] | PG [ppt Br] | PG+SG [ppt Br] |
| CHBr_3 | 0.9 | 1.1 | 0.6 | 0.9 |
| CH_2Br_2 | 2.1 | 4.4 | 1.8 | 3.8 |
| $\text{CHBr}_3 + \text{CH}_2\text{Br}_2$ | 3.0 | 5.5 | 2.4 | 4.7 |

14

15 A detailed comparison of our results over the eastern and western tropical Pacific to results
 16 derived from ATTREX and CONTRAST aircraft measurements and related model calculations
 17 is given in Table 3. Considering that CH_2Br_2 and CHBr_3 contribute >80% of the total SG Br in
 18 the TTL, our SG estimates agree very well with the measurements (Navarro et al., 2015; Werner
 19 et al., 2017; Wales et al., 2018). PG estimates are in general characterized by larger
 20 uncertainties. The PG contribution can be inferred from atmospheric measurements of BrO, the
 21 most abundant Br_y species, and the partitioning of inorganic Br_y derived from a photochemical
 22 model (König et al., 2017; Werner et al., 2017; Wales et al., 2018). Uncertainties in this method
 23 arise from modelling the Br_y partitioning and from uncertainties in measuring BrO and can be
 24 as large as ± 2.1 ppt (e.g., Wales et al., 2018).

1 Our study uses a simplified approach with a prescribed Br_y partitioning including its spatial and
 2 temporal variations. We have carried out sensitivity studies to analyse how variations of the Br_y
 3 partitioning impact the total amount of PG reaching the cold point tropopause (not shown here).
 4 Our studies show that uncertainties of 20% in the partitioning will lead to variations of ± 0.4
 5 ppt in the PG entrainment. Such uncertainties in the Br_y partitioning can result from errors in
 6 the aerosols loading and in the heterogeneous reactions. Distributions of total Br_y and BrO in
 7 p-TOMCAT, the model used to derive the partitioning, have been shown to agree well with in-
 8 situ and satellite observations (Yang et al., 2005; 2010). If the uncertainties in the partitioning
 9 would be as large as 50%, the PG entrainment would show variations of ± 1.1 ppt. Overall the
 10 PG entrainment based on our simplified approach agrees very well (within $\pm 25\%$) with
 11 estimates from other studies derived from BrO measurements and photochemical modelling
 12 (Table 3).

13

14 **Table 3.** Comparison of VLSL source gas (SG) contribution derived from this study and from aircraft
 15 measurements. Product gas (PG) contribution derived from this study and studies linking aircraft
 16 measurements and modelling.

| Br [ppt] | Tropical eastern Pacific | | | Tropical western Pacific | | |
|-----------------------|--------------------------|----------------|-------------------|--------------------------|----------------|-------------------|
| | SG [ppt Br] | PG [ppt Br] | SG+PG [ppt Br] | SG [ppt Br] | PG [ppt Br] | SG+PG [ppt Br] |
| This study | 3 | 2.5 | 5.5 | 2.8 | 2.4 | 5.2 |
| Navarro et al. (2015) | 3 ± 0.4 | 3 ± 1.9 | 6 ± 1.9 | 3.3 ± 0.5 | 2 ± 0.2 | 5.2 ± 0.5 |
| Werner et al. (2017) | 3 ± 0.4 | 2.6 ± 1.0 | 5.6 | | | |
| Wales et al. (2018) | | | | 2.9 ± 0.6 | 2.1 ± 2.1 | 5.0 ± 2.1 |
| König et al. (2017) | | | | | 2.6 ± 0.6 | |

17

1 4 Discussion and summary

2

3 We combine observational data sets, including surface and upper air measurements, with high
4 resolution atmospheric modelling in order to analyse the spatial and temporal variability of
5 VLSL entrainment into the stratosphere. Oceanic CHBr₃ in the TTL, on its way from the marine
6 boundary layer into the stratosphere, shows a very high spatial and temporal variability.
7 Regional maxima with mixing ratios of up to 0.4 to 0.5 ppt are simulated to be over Central
8 America (1) and the Maritime Continent and tropical West Pacific (2), both of which are
9 confirmed by high-altitude aircraft campaigns. The strongest stratospheric CHBr₃ entrainment
10 is projected to occur over the region of India, Bay of Bengal and Arabian Sea (3), however, no
11 data from aircraft campaigns are available to confirm this finding. Other tropical regions with
12 only little convective uplift show smaller mixing ratios, mostly between 0.1 and 0.2 ppt. CHBr₃
13 fields on daily mean or shorter time scales is characterized by pronounced spatial variations
14 with highly localized injections.

15 The modelled CHBr₃ maximum over Central America is caused by the co-occurrence of
16 convectively driven short transport time scales and strong regional sources, with the latter being
17 confirmed by data from various ship campaigns. Moreover, the combined seasonality of
18 transport efficiency and emission strength causes the strong seasonality of CHBr₃ at 17 km over
19 Central America. The model simulations also show a high spatial variability of CHBr₃ with
20 strong latitudinal gradients, which is confirmed by available aircraft campaigns. The
21 comparisons reveal that our model results are similar to the measurements for NH winter, but
22 over- and underestimate (depending on the campaign) observations during NH summer, when
23 the variability is largest. Exceptionally high CHBr₃ observed during the ACCENT campaign
24 is also evident in the model results, but only in the daily and not in the monthly mean values.
25 Given that individual campaigns may not be representative of mean values but may rather
26 describe one side of the large spectrum, differences between model simulations and
27 measurements, such as the ones discussed above, have to be interpreted with caution.

28 The modelled CHBr₃ maximum in the TTL over the West Pacific is centred south of the equator.
29 This distribution cannot be explained by transport times scales, which are similar north and
30 south of the equator and do not reveal strong hemispheric differences. Instead, strong oceanic
31 sources south of equator, prescribed based on limited available measurements, are responsible
32 for the high CHBr₃ mixing ratios in the SH. Measurements in the upper TTL from the ATTREX

1 aircraft campaign show an overall good agreement with model results, but also indicate that the
2 model underestimates CHBr_3 in the tropics. Furthermore, ATTREX measurements did not
3 show any significant gradient between the NH and SH tropics near the tropopause. Given the
4 scarcity of in-situ measurements in the open ocean water of the West Pacific, it may be possible
5 that oceanic emissions estimates used here are too low, especially north of the equator. Future
6 ship campaigns are needed to confirm spatial and temporal differences and to improve existing
7 bottom-up emission climatologies.

8 The overall strongest maximum over India, Bay of Bengal and Arabian Sea is caused by very
9 large local sources. Transport from the ocean surface to 17 km is also efficient, but not strong
10 enough to solely explain the pronounced maxima. No upper air measurements are available to
11 back this upper TTL maximum and oceanic measurements used for the emission scenarios are
12 also scarce. For the global tropical/extratropical distribution of CHBr_3 entrainment, largest
13 uncertainties exist for estimated maxima in the region over India, Bay of Bengal and Arabian
14 Sea. In situ measurements of the oceanic sources and the atmospheric distribution are needed
15 to reduce local uncertainties and confirm global mean values.

16 Our understanding of stratospheric VSLs entrainment is also limited by the fact that currently
17 available emission inventories do not take seasonal variations of oceanic concentrations into
18 account.

19 Interannual variability of stratospheric CHBr_3 entrainment is to a large part driven by the
20 variability of the coupled ocean-atmosphere circulation systems such as ENSO in the Pacific
21 and IOD in the Indian Ocean. Long-term trends of the CHBr_3 entrainment, on the other hand,
22 show a pronounced correlation with the SST trends. Both relations are based on the fact the
23 stratospheric CHBr_3 entrainment is driven by strong sources and convective entrainment, which
24 maximize for high surface temperatures and strong wind speeds. Following the SST trends,
25 long term changes of CHBr_3 entrainment are positive in the West Pacific and Asian monsoon
26 region but negative in the East Pacific. The tropical mean trend accounts for an increase of
27 0.017 ± 0.012 ppt Br/decade resulting in a 10% increase over the 1979-2013 time period. The
28 overall contribution of CHBr_3 and CH_2Br_2 to the stratospheric halogen loading is 4.7 ppt Br
29 with 50% being entrained in form of source gases, and the other 50% being entrained in form
30 of product gases.

31

1

2 **Data availability.** The bromoform and dibromomethane emission inventory data (Ziska et al.,
3 2013) are available at ACP/Pangaea and the FLEXPART model output can be inquired about
4 by contacting the authors.

5 **Author contributions.** ST, KK, and BQ developed the idea for this paper and the model
6 experiments. ST carried out the FLEXPART model calculations and the comparison to the
7 aircraft observations. EA provided aircraft data. FZ compiled the Ziska et al. (2013) climatology
8 for this study. ST wrote the manuscript with contributions from all co-authors. **KK and BQ led**
9 **the ROMIC THREAT project.**

10 **Competing interests.** The authors declare that they have no conflict of interest.

11 **Acknowledgements** This study was carried out within the BMBF project ROMIC THREAT
12 (01LG1217A). ST was funded by ROMIC THREAT (01LG1217A) when compiling the study
13 and by the Deutsche Forschungsgemeinschaft (DFG, German Research Foundation) – TE
14 1134/1 when writing the manuscript. EA was supported by grants from the NASA Upper
15 Atmosphere. The authors are grateful to the ECMWF for making the reanalysis product ERA-
16 Interim available. The authors would like to thank the editor, Jianzhong Ma, and two
17 anonymous reviewers for their helpful comments.

1 **References**

- 2 Aschmann, J., Sinnhuber, B.-M., Atlas, E. L. and Schauffler, S. M.: Modeling the transport of
3 very short-lived substances into the tropical upper troposphere and lower stratosphere,
4 *Atmospheric Chemistry and Physics*, 9(23), 2009.
- 5 Aschmann, J., Sinnhuber, B.-M., Chipperfield, M. P., and Hossaini, R.: Impact of deep
6 convection and dehydration on bromine loading in the upper troposphere and lower
7 stratosphere, *Atmos. Chem. Phys.*, 11, 2671-2687, <https://doi.org/10.5194/acp-11-2671-2011>,
8 2011.
- 9 Austin, J., N., and Butchart, N.: Coupled chemistry-climate model simulations for the period
10 1980 to 2020: ozone depletion and the start of ozone recovery, *Quarterly Journal of the Royal*
11 *Meteorological Society*, 129: 3225–3249, 2006.
- 12 Braesicke, P., Keeble, J., Yang, X., Stiller, G., Kellmann, S., Abraham, N. L., Archibald, A.,
13 Telford, P., and Pyle, J. A.: Circulation anomalies in the Southern Hemisphere and ozone
14 changes, *Atmos. Chem. Phys.*, 13, 10677–10688, doi:10.5194/acp-13-10677-2013, 2013.
- 15 Brinckmann, S., Engel, A., Bönisch, H., Quack, B., and Atlas, E.: Short-lived brominated
16 hydrocarbons – observations in the source regions and the tropical tropopause layer, *Atmos.*
17 *Chem. Phys.*, 12, 1213-1228, doi:10.5194/acp-12-1213-2012, 2012.
- 18 Butler, J. H., King, D. B., Lobert, J. M., Montzka, S. A., Yvon-Lewis, S. A., Hall, B. D.,
19 Warwick, N. J., Mondeel, D. J., Aydin, M. and Elkins, J. W.: Oceanic distributions and
20 emissions of short-lived halocarbons, *Global Biogeochemical Cycles*, 21(1),
21 doi:10.1029/2006GB002732, 2007.
- 22 Carpenter, L.J. and Reimann, S. (Lead Authors), J.B. Burkholder, C. Clerbaux, B.D. Hall, R.
23 Hossaini, J.C. Laube, and S.A. Yvon-Lewis, *Ozone-Depleting Substances (ODSs) and Other*
24 *Gases of Interest to the Montreal Protocol*, Chapter 1 in *Scientific Assessment of Ozone*
25 *Depletion: 2014*, Global Ozone Research and Monitoring Project–Report No. 55, World
26 Meteorological Organization, Geneva, Switzerland, 2014.
- 27 Chipperfield, M. P.: New version of the TOMCAT/SLIMCAT off-line chemical transport
28 model: Intercomparison of stratospheric tracer experiments, *Quarterly Journal of the Royal*
29 *Meteorological Society*, 132(617), 1179–1203, doi:10.1256/qj.05.51, 2006.
- 30 Dee, D. P., Uppala, S. M., Simmons, A. J., Berrisford, P., Poli, P., Kobayashi, S., Andrae, U.,
31 Balmaseda, M. A., Balsamo, G., Bauer, P., Bechtold, P., et al.: The ERA-Interim reanalysis:
32 configuration and performance of the data assimilation system, *Quarterly Journal of the Royal*
33 *Meteorological Society*, 137(656), 553–597, doi:10.1002/qj.828, 2011.
- 34 Dorf, M., Butz, A., Camy-Peyret, C., Chipperfield, M. P., Kritten, L., and Pfeilsticker, K.:
35 Bromine in the tropical troposphere and stratosphere as derived from balloon-borne BrO
36 observations, *Atmos. Chem. Phys.*, 8, 7265-7271, doi:10.5194/acp-8-7265-2008, 2008.

- 1 Engel, A., Rigby, M. (Lead A., Burkholder, J. B., Fernandez, R. P., Froidevaux, L., Hall, B. D.,
2 Hossaini, R., Saito, T., Vollmer, M. K. and Yao, B.: Update on Ozone-Depleting Substances
3 (ODSs) and Other Gases of Interest to the Montreal Protocol, Chapter 1, in Scientific
4 Assessment of Ozone Depletion: 2018, Global Ozone Research and Monitoring Project –
5 Report No. 58., 2018.
- 6 Fernandez, R. P., Salawitch, R. J., Kinnison, D. E., Lamarque, J.-F., and Saiz-Lopez, A.:
7 Bromine partitioning in the tropical tropopause layer: implications for stratospheric in-
8 Atmos. Chem. Phys., 14, 13391-13410, [https://doi.org/10.5194/acp-14-13391-](https://doi.org/10.5194/acp-14-13391-2014) 2014, 2014.
- 9 Fiehn, A., Quack, B., Hepach, H., Fuhlbrügge, S., Tegtmeier, S., Toohey, M., Atlas, E., and
10 Krüger, K.: Delivery of halogenated very short-lived substances from the west Indian Ocean to
11 the stratosphere during the Asian summer monsoon, Atmos. Chem. Phys., 17, 6723-6741,
12 <https://doi.org/10.5194/acp-17-6723-2017>, 2017.
- 13 Fiehn, A., Quack, B., Marandino, C. A., and Krüger, K., Transport variability of very short
14 lived substances from the West Indian Ocean to the stratosphere. Journal of Geophysical
15 Research: Atmospheres, 123, 5720– 5738. <https://doi.org/10.1029/2017JD027563>, 2018a.
- 16 Fiehn, A., Quack, B., Stemmler, I., Ziska, F., and Krüger, K.: Importance of seasonally resolved
17 oceanic emissions for bromoform delivery from the tropical Indian Ocean and west Pacific to
18 the stratosphere, Atmos. Chem. Phys., 18, 11973–11990, [https://doi.org/10.5194/acp-18-](https://doi.org/10.5194/acp-18-11973-2018)
19 11973-2018, 2018b.
- 20 Forster, C., Stohl, A. and Seibert, P.: Parameterization of Convective Transport in a Lagrangian
21 Particle Dispersion Model and Its Evaluation, Journal of Applied Meteorology and
22 Climatology, 46(4), 403–422, doi:10.1175/JAM2470.1, 2007.
- 23 Forster, C., Wandinger, U., Wotawa, G., James, P., Mattis, I., Althausen, D., Simmonds, P.,
24 O’Doherty, S., Jennings, S. G., Kleefeld, C., Schneider, J., et al.: Transport of boreal forest fire
25 emissions from Canada to Europe, Journal of Geophysical Research, 106(D19), 22887,
26 doi:10.1029/2001JD900115, 2001.
- 27 Fuhlbrügge, S., Quack, B., Tegtmeier, S., Atlas, E., Hepach, H., Shi, Q., Raimund, S., and
28 Krüger, K.: The contribution of oceanic halocarbons to marine and free tropospheric air over
29 the tropical West Pacific, Atmos. Chem. Phys., 16, 7569-7585, [https://doi.org/10.5194/acp-16-](https://doi.org/10.5194/acp-16-7569-2016)
30 7569-2016, 2016.
- 31 Hegerl, G.C., F. W. Zwiers, P. Braconnot, N.P. Gillett, Y. Luo, J.A. Marengo Orsini, N.
32 Nicholls, J.E. Penner and P.A. Stott: Understanding and Attributing Climate Change. In:
33 Climate Change 2007: The Physical Science Basis. Contribution of Working Group I to the
34 Fourth Assessment Report of the Intergovernmental Panel on Climate Change [Solomon, S., D.
35 Qin, M. Manning, Z. Chen, M. Marquis, K.B. Averyt, M. Tignor and H.L. Miller (eds.)].
36 Cambridge University Press, Cambridge, United Kingdom and New York, NY, USA, 2007

- 1 Hepach, H., Quack, B., Tegtmeier, S., Engel, A., Bracher, A., Fuhlbrügge, S., Galgani, L.,
2 Atlas, E. L., Lampel, J., Frieß, U., and Krüger, K.: Biogenic halocarbons from the Peruvian
3 upwelling region as tropospheric halogen source, *Atmos. Chem. Phys.*, 16, 12219-12237,
4 <https://doi.org/10.5194/acp-16-12219-2016>, 2016.
- 5 Hossaini, R., Chipperfield, M. P., Monge-Sanz, B. M., Richards, N. A. D., Atlas, E., and Blake,
6 D. R.: Bromoform and dibromomethane in the tropics: a 3-D model study of chemistry and
7 transport, *Atmos. Chem. Phys.*, 10, 719–735, <https://doi.org/10.5194/acp-10-719-2010>, 2010.
- 8 Hossaini, R., Chipperfield, M. P., Dhomse, S., Ordóñez, C., Saiz-Lopez, A., Abraham, N. L.,
9 Archibald, A. T., Braesicke, P., Telford, P., and Warwick, N.: Modelling future changes to the
10 stratospheric source gas injection of biogenic bromocarbons, *Geophys. Res. Lett.*, 39, L20813,
11 doi: 10.1029/2012GL053401, 2012a.
- 12 Hossaini, R., Chipperfield, M. P., Feng, W., Breider, T. J., Atlas, E., Montzka, S. A., Miller, B.
13 R., Moore, F. and Elkins, J.: The contribution of natural and anthropogenic very short-lived
14 species to stratospheric bromine, *Atmospheric Chemistry and Physics*, 12(1), 371–380,
15 doi:10.5194/acp-12-371-2012, 2012b.
- 16 Hossaini, R., Mantle, H., Chipperfield, M. P., Montzka, S. A., Hamer, P., Ziska, F., Quack, B.,
17 Krüger, K., Tegtmeier, S., Atlas, E., Sala, S., Engel, A., Bönisch, H., Keber, T., Oram, D., Mills,
18 G., Ordóñez, C., Saiz-Lopez, A., Warwick, N., Liang, Q., Feng, W., Moore, F., Miller, B. R.,
19 Marécal, V., Richards, N. A. D., Dorf, M., and Pfeilsticker, K.: Evaluating global emission
20 inventories of biogenic bromocarbons, *Atmos. Chem. Phys.*, 13, 11819-11838,
21 doi:10.5194/acp-13-11819-2013, 2013.
- 22 Hossaini, R., Chipperfield, M. P., Montzka, S. A., Rap, A., Dhomse, S., and Feng, W.:
23 Efficiency of short-lived halogens at influencing climate through depletion of stratospheric
24 ozone, *Nat. Geosci.*, 8, 186–190, doi:10.1038/ngeo2363, 2015.
- 25 Hossaini, R., Patra, P. K., Leeson, A. A., Krysztofiak, G., Abraham, N. L., Andrews, S. J.,
26 Archibald, A. T., Aschmann, J., Atlas, E. L., Belikov, D. A., Bönisch, H., Carpenter, L. J.,
27 Dhomse, S., Dorf, M., Engel, A., Feng, W., Fuhlbrügge, S., Griffiths, P. T., Harris, N. R. P.,
28 Hommel, R., Keber, T., Krüger, K., Lennartz, S. T., Maksyutov, S., Mantle, H., Mills, G. P.,
29 Miller, B., Montzka, S. A., Moore, F., Navarro, M. A., Oram, D. E., Pfeilsticker, K., Pyle, J.
30 A., Quack, B., Robinson, A. D., Saikawa, E., Saiz-Lopez, A., Sala, S., Sinnhuber, B.-M.,
31 Taguchi, S., Tegtmeier, S., Lidster, R. T., Wilson, C., and Ziska, F.: A multi-model
32 intercomparison of halogenated very short-lived substances (TransCom-VSLS): linking
33 oceanic emissions and tropospheric transport for a reconciled estimate of the stratospheric
34 source gas injection of bromine, *Atmos. Chem. Phys.*, 16, 9163-9187, doi:10.5194/acp-16-
35 9163-2016, 2016.
- 36 Ko, M.K.W. and Poulet, G. (Lead Authors) Blake, D.R., Boucher, O., Burkholder, J.H., Chin,
37 M., Cox, R.A., George, C., Graf, H.-F., Holton, J.R., Jacob, D.J., Law, K.S., Lawrence, M.G.,
38 Midgley, P.M., Seakins, P.W., Shallcross, D.E., Strahan, S.E., Wuebbles, D.J., and Yokouchi,
39 Y. (2002) Very short-lived halogen and sulfur substances. Chapter 2 in Scientific Assessment

- 1 of Ozone Depletion: 2002 Global Ozone Research and Monitoring Project–Report No. 47,
2 World Meteorological Organization, Geneva, Switzerland, 2003.
- 3 Krüger, K., Tegtmeier, S. and Rex, M.: Variability of residence time in the Tropical Tropopause
4 Layer during Northern Hemisphere winter, *Atmos. Chem. Phys.*, 9(18), 6717–6725, 2009.
- 5 Liang, Q., Stolarski, R. S., Kawa, S. R., Nielsen, J. E., Douglass, A. R., Rodriguez, J. M., Blake,
6 D. R., Atlas, E. L., and Ott, L. E.: Finding the missing stratospheric Bry: a global modeling
7 study of CHBr₃ and CH₂Br₂, *Atmos. Chem. Phys.*, 10, 2269–2286, doi:10.5194/acp-10-2269-
8 2010, 2010.
- 9 Liang, Q., Atlas, E., Blake, D., Dorf, M., Pfeilsticker, K., and Schauffler, S.: Convective
10 transport of very short lived bromocarbons to the stratosphere, *Atmos. Chem. Phys.*, 14, 5781-
11 5792, <https://doi.org/10.5194/acp-14-5781-2014>, 2014.
- 12 Luo, J. J., W. Sasak ia, and Y. Masumoto: Indian Ocean warming modulates Pacific climate
13 change, *Proc. Natl. Acad. Sci. U.S.A.*, 109, 18,701–18,706, doi:10.1073/pnas.1210239109,
14 2012.
- 15 Marandino, C. A., Tegtmeier, S., Krüger, K., Zindler, C., Atlas, E. L., Moore, F., and Bange,
16 H. W.: Dimethylsulphide (DMS) emissions from the western Pacific Ocean: a potential marine
17 source for stratospheric sulphur?, *Atmos. Chem. Phys.*, 13, 8427–8437,
18 <https://doi.org/10.5194/acp-13-8427-2013>, 2013.
- 19 McLinden, C. A., Haley, C. S., Lloyd, N. D., Hendrick, F., Rozanov, A., Sinnhuber, B.-M.,
20 Goutail, F., Degenstein, D. A., Llewellyn, E. J., Sioris, C. E., Van Rozendael, M., Pommereau,
21 J. P., Lotz, W., and Burrows, J. P.: Odin/OSIRIS observations of stratospheric BrO: Retrieval
22 methodology, climatology, and inferred Bry, *J. Geophys. Res.-Atmos.*, 115, D15308,
23 doi:10.1029/2009JD012488, 2010.
- 24 Navarro, M. A., Atlas, E. L., Saiz-Lopez, A., Rodriguez-Lloveras, X., Kinnison, D. E.,
25 Lamarque, J.-F., Tilmes, S., Filus, M., Har- ris, N. R., and Meneguz, E.: Airborne measurements
26 of organic bromine compounds in the Pacific tropical tropopause layer, *P. Natl. Acad. Sci. USA*,
27 112, 13789–13793, 2015.
- 28 Nightingale, P. D., Malin, G., Law, C. S., Watson, A. J., Liss, P. S., Liddicoat, M. I., Boutin, J.
29 and Upstill-Goddard, R. C.: In situ evaluation of air-sea gas exchange parameterizations using
30 novel conservative and volatile tracers, *Global Biogeochemical Cycles*, 14(1), 373–387,
31 doi:10.1029/1999GB900091, 2000.
- 32 Ordóñez, C., Lamarque, J.-F., Tilmes, S., Kinnison, D. E., Atlas, E. L., Blake, D. R., Sousa
33 Santos, G., Brasseur, G. and Saiz-Lopez, A.: Bromine and iodine chemistry in a global
34 chemistry-climate model: description and evaluation of very short-lived oceanic sources,
35 *Atmospheric Chemistry and Physics*, 12(3), 1423–1447, doi:10.5194/acp-12-1423-2012, 2012.

- 1 Pisso, I., Haynes, P. H., and Law, K. S.: Emission location dependent ozone depletion potentials
2 for very short-lived halogenated species, *Atmos. Chem. Phys.*, 10, 12025–12036,
3 doi:10.5194/acp-10-12025-2010, 2010.
- 4 Pyle, J. A., N. Warwick, X. Yang, P. J. Young, and G. Zeng: Climate/chemistry feedbacks and
5 biogenic emissions, *Philos. Trans. R. Soc. A*, 365(1856), 1727–1740,
6 doi:10.1098/rsta.2007.2041, 2007.
- 7 Quack, B., Wallace, D.W.R.: Air-sea flux of bromoform: Controls, rates, and implications.
8 *Global Biogeochemical Cycles*, 17 (1), art. no.-GB1023, 2003.
- 9 Quack, B., E. Atlas, G. Petrick, and D. W. R. Wallace: Bromoform and dibromomethane above
10 the Mauritanian upwelling: Atmospheric distributions and oceanic emissions, *J. Geophys. Res.*,
11 112(D9), D09312, doi:10.1029/2006JD007614, 2007.
- 12 Randel, W. J., Park, M., Emmons, L., Kinnison, D., Bernath, P., Walker, K. A., Boone, C., and
13 Pumphrey, H.: Asian Monsoon Transport of Pollution to the Stratosphere, *Science*, 328, 611–
14 613, doi:10.1126/science.1182274, 2010.
- 15 Saji, N. H., Goswami, B. N., Vinayachandran, P. N., and Yamagata, T.: A dipole made in the
16 Tropical Indian Ocean. *Nature*. 401. 360-3. 10.1038/43854, 1999.
- 17 Salawitch, R. J.: Atmospheric chemistry: biogenic bromine, *Nature*, 439, 275–277, 2006.
- 18 Salawitch, Ross J. (Lead Author), David W. Fahey, Michaela I. Hegglin, Laura A. McBride,
19 Walter R. Tribett, Sarah J. Doherty, *Twenty Questions and Answers About the Ozone Layer:
20 2018 Update, Scientific Assessment of Ozone Depletion: 2018*, 84 pp., World Meteorological
21 Organization, Geneva, Switzerland, 2019.
- 22 Schmidt, J. A., et al., Modeling the observed tropospheric BrO background: Importance of
23 multiphase chemistry and implications for ozone, OH, and mercury, *J. Geophys. Res. Atmos.*,
24 121, 11,819– 11,835, doi:10.1002/2015JD024229, 2016.
- 25 Simmons, A. J., Poli, P. , Dee, D. P., Berrisford, P. , Hersbach, H. , Kobayashi, S. and Peubey,
26 C.: Estimating low-frequency variability and trends in atmospheric temperature using ERA-
27 Interim. *Q.J.R. Meteorol. Soc.*, 140: 329-353. doi:10.1002/qj.2317, 2014.
- 28 Sinnhuber, B., and S. Meul: Simulating the impact of emissions of brominated very short lived
29 substances on past stratospheric ozone trends. *Geophys. Res. Lett.*, 42, 2449–2456. doi:
30 10.1002/2014GL062975, 2015.
- 31 Sioris, C. E., et al.: Latitudinal and vertical distribution of bromine monoxide in the lower
32 stratosphere from Scanning Imaging Absorption Spectrometer for Atmospheric Chartography
33 limb scattering measurements, *J. Geophys. Res.*, 111, D14301, doi: 10.1029/2005JD006479,
34 2006.

- 1 Stemmler, I., Hense, I., and Quack, B.: Marine sources of bromoform in the global open ocean
2 – global patterns and emissions, *Biogeosciences*, 12, 1967-1981, [https://doi.org/10.5194/bg-12-](https://doi.org/10.5194/bg-12-1967-2015)
3 1967-2015, 2015.
- 4 Stohl, A., Forster, C., Frank, A., Seibert, P. and Wotawa, G.: Technical note: The Lagrangian
5 particle dispersion model FLEXPART version 6.2, *Atmospheric Chemistry and Physics*, 5(9),
6 2005.
- 7 Stohl, A., Hittenberger, M., and Wotawa, G.: Validation of the Lagrangian particle dispersion
8 model FLEXPART against large-scale tracer experiment data, *Atmos. Environ.*, 32, 4245–
9 4264, 1998.
- 10 Stohl, A. and Thomson, D. J.: A density correction for Lagrangian particle dispersion models,
11 *BOUNDARY-LAYER METEOROLOGY*, 90(1), 155–167, doi:10.1023/A:1001741110696,
12 1999.
- 13 Stohl, A. and Trickl, T.: A textbook example of long-range transport: Simultaneous observation
14 of ozone maxima of stratospheric and North American origin in the free troposphere over
15 Europe, *Journal of Geophysical Research*, 104(D23), 30445, doi:10.1029/1999JD900803,
16 1999.
- 17 Stohl, A., Sodemann, H., Eckhardt, S., Frank, A., Seibert, P., and Wotawa, G.: The Lagrangian
18 particle dispersion model FLEXPART version 8.2, Tech. rep., Norwegian Institute of Air Re-
19 search (NILU), Kjeller, Norway, available at: <http://flexpart.eu/>, last access: 2 April 2020, 2010.
- 20 Tegtmeier, S., Krüger, K., Quack, B., Atlas, E. L., Pisso, I., Stohl, A. and Yang, X.: Emission
21 and transport of bromocarbons: from the West Pacific ocean into the stratosphere, *Atmospheric*
22 *Chemistry and Physics*, 12(22), 10633–10648, doi:10.5194/acp-12-10633-2012, 2012.
- 23 Tegtmeier, S., Krüger, K., Quack, B., Atlas, E., Blake, D. R., Boenisch, H., Engel, A., Hepach,
24 H., Hossaini, R., Navarro, M. A., Raimund, S., Sala, S., Shi, Q., and Ziska, F.: The contribution
25 of oceanic methyl iodide to stratospheric iodine, *Atmos. Chem. Phys.*, 13, 11869-11886,
26 <https://doi.org/10.5194/acp-13-11869-2013>, 2013.
- 27 Tegtmeier, S., Ziska, F., Pisso, I., Quack, B., Velders, G. J. M., Yang, X., and Krüger, K.:
28 Oceanic bromoform emissions weighted by their ozone depletion potential, *Atmos. Chem.*
29 *Phys.*, 15, 13647-13663, doi:10.5194/acp-15-13647-2015, 2015.
- 30 Tegtmeier, S., Anstey, J., Davis, S., Dragani, R., Harada, Y., Ivanciu, I., Pilch Kedzierski, R.,
31 Krüger, K., Legras, B., Long, C., Wang, J. S., Wargan, K., and Wright, J. S.: Temperature and
32 tropopause characteristics from reanalyses data in the tropical tropopause layer, *Atmos. Chem.*
33 *Phys.*, 20, 753–770, <https://doi.org/10.5194/acp-20-753-2020>, 2020.
- 34 Tissier, A.-S. and Legras, B.: Convective sources of trajectories traversing the tropical
35 tropopause layer, *Atmos. Chem. Phys.*, 16, 3383–3398, doi:10.5194/acp-16-3383-2016, 2016.

- 1 Wales, P. A., Salawitch, R. J., Nicely, J. M., Anderson, D. C., Canty, T. P., Baidar, S., et al.,
2 Stratospheric injection of brominated very short-lived substances: Aircraft observations in the
3 Western Pacific and representation in global models. *Journal of Geophysical Research:*
4 *Atmospheres*, 123. [https://doi.org/ 10.1029/2017JD027978](https://doi.org/10.1029/2017JD027978), 2018.
- 5 Wang, B., J. Liu, H. J. Kim, P. J. Webster, and S. Y. Yim: Recent change of the global monsoon
6 precipitation (1979–2008), *Clim. Dyn.*, 39, 1123–1135, doi:10.1007/s00382-011-1266-z, 2012.
- 7 Warwick, N. J., J. A. Pyle, G. D. Carver, X. Yang, N. H. Savage, F. M. O'Connor, and R. A.
8 Cox: Global modeling of biogenic bromocarbons, *J. Geophys. Res.*, 111, D24305,
9 doi:10.1029/2006JD007264, 2006.
- 10 Werner, B., Stutz, J., Spolaor, M., Scalone, L., Raecke, R., Festa, J., Colosimo, S. F., Cheung,
11 R., Tsai, C., Hossaini, R., Chipperfield, M. P., Taverna, G. S., Feng, W., Elkins, J. W., Fahey,
12 D. W., Gao, R.-S., Hints, E. J., Thornberry, T. D., Moore, F. L., Navarro, M. A., Atlas, E.,
13 Daube, B. C., Pittman, J., Wofsy, S., and Pfeilsticker, K.: Probing the subtropical lowermost
14 stratosphere and the tropical upper troposphere and tropopause layer for inorganic bromine,
15 *Atmos. Chem. Phys.*, 17, 1161–1186, <https://doi.org/10.5194/acp-17-1161-2017>, 2017.
- 16 Wolter, K. and Timlin, M. S.: El Niño/Southern Oscillation behaviour since 1871 as diagnosed
17 in an extended multivariate ENSO index (MEI.ext). *Int. J. Climatol.*, 31: 1074-1087.
18 doi:10.1002/joc.2336, 2011.
- 19 Yamamoto, H., Yokouchi, Y., Otsuki, A., and Itoh, H.: Depth profiles of volatile halogenated
20 hydrocarbons in seawater in the Bay of Bengal, *Chemosphere*, 45, 371–377,
21 doi:10.1016/s0045-6535(00)00541-5, 2001.
- 22 Yang, X., Cox, R. A., Warwick, N. J., Pyle, J. A., Carver, G. D., O'Connor, F. M., and Savage,
23 N. H.: Tropospheric bromine chemistry and its impacts on ozone: A model study, *J. Geophys.*
24 *Res.*, 110, D23311, doi:10.1029/2005JD006244, 2005.
- 25 Yang, X., Pyle, J. A., Cox, R. A., Theys, N., and Van Roozendael, M.: Snow-sourced bromine
26 and its implications for polar tropospheric ozone, *Atmos. Chem. Phys.*, 10, 7763-7773,
27 doi:10.5194/acp-10-7763-2010, 2010.
- 28 Yang, X., Abraham, N. L., Archibald, A. T., Braesicke, P., Keeble, J., Telford, P. J., Warwick,
29 N. J., and Pyle, J. A.: How sensitive is the recovery of stratospheric ozone to changes in
30 concentrations of very short-lived bromocarbons?, *Atmos. Chem. Phys.*, 14, 10431-10438,
31 doi:10.5194/acp-14-10431-2014, 2014.
- 32 Ziska, F., Quack, B., Abrahamsson, K., Archer, S. D., Atlas, E., Bell, T., Butler, J. H.,
33 Carpenter, L. J., Jones, C. E., Harris, N. R. P., Hepach, H., et al.: Global sea-to-air flux
34 climatology for bromoform, dibromomethane and methyl iodide, *Atmospheric Chemistry and*
35 *Physics Discussions*, 13(2), 5601–5648, doi:10.5194/acpd-13-5601-2013, 2013.

1 Ziska, F., Quack, B., Tegtmeier, S., Stemmler, I., and Krüger, K.: Future emissions of marine
2 halogenated very-short lived substances under climate change. *Journal of Atmospheric*
3 *Chemistry*, 74: 245. <https://doi.org/10.1007/s10874-016-9355-3>, 2017.

4